

BIROn - Birkbeck Institutional Research Online

Meschis, Marco and Roberts, Gerald P. and Robertson, Jennifer and Briant, Rebecca M. (2018) The relationships between regional Quaternary uplift, deformation across active normal faults and historical seismicity in the upper plate of subduction zones: The Capo D'Orlando Fault, NE Sicily. *Tectonics* 37 (5), pp. 1231-1255. ISSN 0278-7407.

Downloaded from: <https://eprints.bbk.ac.uk/id/eprint/22605/>

Usage Guidelines:

Please refer to usage guidelines at <https://eprints.bbk.ac.uk/policies.html>

or alternatively

contact lib-eprints@bbk.ac.uk.

1 **The relationships between regional Quaternary uplift, deformation across active normal**
2 **faults and historical seismicity in the upper plate of subduction zones: The Capo**
3 **D'Orlando Fault, NE Sicily.**

4

5 M. Meschis^{1*}, G.P. Roberts¹, J. Robertson¹ and R.M. Briant².

6 ¹Department of Earth and Planetary Sciences, Birkbeck, University of London, WC1E 7HX, UK.

7 ²Department of Geography, Environment and Development Studies, Birkbeck, University of London, WC1E
8 7HX, UK

9

10 **Abstract**

11

12 In order to investigate deformation within the upper plate of the Calabrian subduction zone
13 we have mapped and modelled a sequence of Late Quaternary palaeoshorelines tectonically-deformed
14 by the Capo D'Orlando normal fault, NE Sicily, which forms part of the actively deforming Calabrian
15 Arc. In addition to the 1908 Messina Strait earthquake (Mw 7.1), this region has experienced
16 damaging earthquakes, possibly on the Capo D'Orlando Fault, however, it is not considered by some
17 to be a potential seismogenic source. Uplifted Quaternary palaeoshorelines are preserved on the
18 hangingwall of the Capo D'Orlando Fault, indicating that hangingwall subsidence is counteracted by
19 regional uplift, likely because of deformation associated with subduction/collision. We attempt to
20 constrain the relationship between regional uplift, crustal extensional processes and historical
21 seismicity, and we quantify both the normal and regional deformation signals. We report uplift
22 variations along the strike of the fault and use a synchronous correlation technique to assign ages to
23 palaeoshorelines, facilitating calculation of uplift rates and the fault throw-rate. Uplift rates in the
24 hangingwall increase from 0.4 mm/yr in the centre of the fault to 0.89 mm/yr beyond its SW fault tip,
25 suggesting 0.5 mm/yr of fault related subsidence, which implies a throw-rate of 0.63 ± 0.02 mm/yr,
26 and significant seismic hazard. Overall, we emphasise that upper plate extension and related vertical
27 motions complicate the process of deriving information on the subduction/collision process, such as

28 coupling and slip distribution on the subduction interface, parameters that are commonly inferred for
29 other subduction zones without considering upper plate deformation.

30

31 **Keywords:** Quaternary; Palaeoshorelines; Marine terraces; Sea level changes; Synchronous
32 correlation method; Uplift rate; Normal faulting, Fault slip-rate; DISS; Crustal deformation

33

34 *Corresponding author.

35 *E-mail address: marco.meschis.14@ucl.ac.uk (M. Meschis)*

36

37 **1. Introduction**

38

39 Data on coastal uplift in the upper plate of subduction zone are commonly used to infer the slip
40 distributions and gain insight into the processes of coupling along the subduction interface and mantle
41 upwelling [McCloskey *et al.*, 2005; Meltzner *et al.*, 2006; Nalbant *et al.*, 2013; Nic Bhloscaidh *et al.*,
42 2015; D'Agostino *et al.*, 2001; Faure Walker *et al.*, 2012; Faccenna *et al.*, 2014]. This paper
43 emphasises that there is a growing body of evidence that the upper plates of subduction zones can also
44 be deformed by active normal faults. This evidence is widespread for example from central Greece
45 and Crete [Armijo *et al.*, 1992; Papanikolaou *et al.*, 2006; Gallen *et al.*, 2014], south America
46 [Saillard *et al.*, 2011; Binnie *et al.*, 2016], New Zealand [Nicol and Beavan, 2003], Japan [Hasegawa
47 *et al.*, 2000] and southern Italy [Monaco and Tortorici, 2000; Jacques *et al.*, 2001; Spampinato *et al.*,
48 2012; Roberts *et al.*, 2013]. Deformation related to normal faulting must be removed if the observed
49 coastal uplift is to be used to constrain both the slip-distribution on the subduction interface and
50 mantle dynamics-related topography.

51 Long-term crustal extension processes occurring in Calabria and NE Sicily have been
52 accommodated by active normal faults that have been deforming palaeoshorelines through the Late
53 Quaternary [Monaco and Tortorici, 2000; Jacques *et al.*, 2001; Catalano and De Guidi, 2003; Giunta
54 *et al.*, 2012; Roberts *et al.*, 2013]. The locations of historical damaging earthquakes from Italian

55 catalogues [*Guidoboni et al.*, 2007; *Stucchi et al.*, 2013] lie close to these mapped normal faults
56 [*Monaco and Tortorici*, 2000; *Galli et al.*, 2008; *Roberts et al.*, 2013] . Potential seismogenic sources
57 have been collated within the Database of Individual Seismogenic Source (DISS) [*Basili et al.*, 2008],
58 providing a base from which to define the geography of seismic hazard in Italy. However, we ask
59 whether the locations of all active normal faults that can be considered to be candidate seismogenic
60 sources are known. For example, even though two well-documented medium-magnitude historical
61 seismic events have been reported [*Guidoboni et al.*, 2007] around the Capo D’Orlando area, in NE
62 Sicily, only a few studies [*Scicchitano et al.*, 2011; *Giunta et al.*, 2012] have attempted to identify
63 plausible potential seismogenic sources, such as the Capo D’Orlando Fault. These authors recognised
64 that Quaternary palaeoshorelines are tilted and hence deformed by the Capo D’Orlando Fault,
65 suggesting the fault is active. However, the results are considered equivocal by some, for example
66 because no active faults are reported in this location within the DISS [*Basili et al.*, 2008] . In this
67 study, we investigate whether the Capo D’Orlando Fault reported by *Scicchitano et al.* [2011] and
68 *Giunta et al.*, [2012] should be added to the DISS.

69 A quantitative understanding of Late Quaternary upper-crustal vertical movements such as
70 tectonic uplift and/or subsidence and their associated slip-rates on active normal faults within a plate
71 boundary region is fundamental to long-term seismic hazard assessment [*Roberts et al.*, 2013]. We
72 take into account the notion that any evidence of fault movement since the Middle/Late Pleistocene
73 has been accepted by some as the definition of an “active fault” [*Yeats*, 2012; *Chapman et al.*, 2014].
74 Therefore, we study the long-term deformation since the Middle Pleistocene by investigating
75 sequences of deformed palaeoshorelines, which can be used to (i) help differentiate between transitory
76 strain-rates associated with temporal earthquake clustering, and (ii) judge how long-term strain-rates
77 measured over many seismic cycles relate to those measured over shorter timescales [*Yeats and*
78 *Prentice*, 1996; *Ward*, 1998; *Friedrich et al.*, 2003; *Papanikolaou et al.*, 2005; *Faure Walker et al.*,
79 2010; *Roberts et al.*, 2013].

80 The approach that we have taken is to examine differential uplift across the candidate active
81 fault in question [*Massonnet et al.*, 1993; *Massonnet and Feigl*, 1995; *Armijo et al.*, 1996; *Roberts et*
82 *al.*, 2009, 2013; *Walters et al.*, 2009; *Papanikolaou et al.*, 2010]. In particular, we focus our attention

83 on the 15 km onshore section of the NE–SW oriented Capo D’Orlando Fault [*Scicchitano et al.*, 2011;
84 *Giunta et al.*, 2012]. We conduct new mapping alongside a review of ages for previously-mapped
85 palaeoshorelines outcropping on the hangingwall of the Capo D’Orlando Fault. The age review is
86 conducted by attempting to correlate palaeoshorelines that are unevenly spaced in elevation with
87 glacio-eustatic sea-level highstands that are unevenly spaced in time through iteration of the uplift rate
88 history [*Roberts et al.*, 2009, 2013]. This work (i) quantifies uplift rates values, (ii) investigates along-
89 strike variation in uplift rate, which if correlated with the fault offset and fault-tip locations, will
90 confirm Quaternary activity on the fault, (iii) investigates rates of tilting for palaeoshorelines along
91 the strike of the fault to define displacement gradients, and (iv) estimates the associated slip-rate
92 through correlation between offset palaeoshorelines preserved in the hangingwall and footwall, which
93 has fundamental tectonic and seismic hazard implications [*Cowie et al.*, 2012]. We investigate the
94 above by mapping the inner edges of marine terraces (palaeoshorelines) both through detailed
95 topographic surveying using a 10-m resolution Digital Elevation Model (DEM) [*Tarquini et al.*, 2007,
96 2012] and fieldwork, seeking to confirm the reliability of the mapping by *Giunta et al.* [2012]. We
97 then correlate our mapped inner edge elevations with glacio-eustatic sea-level highstands since the
98 Middle Pleistocene, by iterating the uplift-rate. We assess the robustness of our correlations between
99 multiple mapped palaeoshorelines and multiple sea-level highstands through linear regression
100 analysis. Finally, we discuss our results in terms of local and regional tectonic implications and
101 seismic hazard assessment within the Ionian subduction zone and the associated Plio-Pleistocene
102 regional extensional processes, which are accommodated by several upper crustal active normal faults
103 potentially producing damaging earthquakes.

104

105 **2. Background**

106

107 *2.1. Geological background*

108 The study area lies in the southernmost part of the Calabrian Arc, which forms the link
109 between the NW–SE oriented southern Apennines thrust belt in mainland Italy and the E-W oriented

110 Maghrebide chain in northern Sicily [*Tortorici et al.*, 1995] (Figure 1). As a response to Neogene–
111 Quaternary Africa–Eurasia continental collision and the ongoing southeastwardly subduction of the
112 Ionian plate beneath Calabria, probably associated with the opening of Tyrrhenian Extensional Basin
113 [*Rehault et al.*, 1984; *Malinverno and Ryan*, 1986; *Dewey et al.*, 1989; *Selvaggi and Chiarabba*, 1995;
114 *Gutscher et al.*, 2017], the Calabrian Arc represents one of the most tectonically active regions in the
115 Mediterranean. Since the Pliocene, structural features produced by Neogene shortening have been
116 fragmented by extensional faults producing geomorphological landscapes characterised by structural
117 highs and sedimentary basins [*Barone et al.*, 1982; *Ghisetti and Vezzani*, 1982; *Trincardi and*
118 *Zitellini*, 1987; *Kastens et al.*, 1988; *Pepe et al.*, 2000, 2003].

119 Since the Pliocene–Early Pleistocene, Calabria and NE Sicily have been affected by active
120 normal faulting mostly on the Tyrrhenian side and within the Messina Strait between Sicily and
121 Calabria, uplifting and deforming Quaternary marine deposits in response to NW–SE regional
122 extension [*Monaco and Tortorici*, 2000], including near Capo D’Orlando town [*Giunta et al.*, 2012].
123 Some geoscientists have proposed a cessation or slowing of the roll-back process and associated
124 extension within the Tyrrhenian Basin due to the de-coupling of the Ionian slab from the Calabrian
125 Arc since 700 ky [*Gvirtzman and Nur*, 1999; *Wortel and Spakman*, 2000; *Goes et al.*, 2004;
126 *Serpelloni et al.*, 2005, 2007; *Palano et al.*, 2012]. This suggested slab detachment process is thought
127 to have produced both the sinking of the slab itself, with related isostatic rebound and lithospheric
128 tearing-related faulting near the SW and NE tips of the NW-dipping Ionian slab, producing flow of
129 mantle material through slab windows just beneath the crust of the Calabrian Arc. These processes
130 have produced significant uplift and crustal extension within the upper plate of the Ionian subduction
131 zone through the Middle Pleistocene [*Gvirtzman and Nur*, 1999; *Faccenna et al.*, 2011].

132 Ongoing extension and uplift is confirmed by (i) GPS investigations, which demonstrate an
133 extension rate of 2 mm/yr with local uplift rates as high as 0.5-1.0 mm/yr [*Serpelloni et al.*, 2005;
134 *Mastrolembo Ventura et al.*, 2014; *Scarfi et al.*, 2016a; *Chiarabba and Palano*, 2017], and (ii)
135 historical seismicity in the overriding plate [*Monaco and Tortorici*, 2000]. Historical damaging
136 earthquakes have been reported in and around the study area [*Guidoboni et al.*, 2007; *Stucchi et al.*,
137 2013]. In particular, two medium historical seismic events have been located within the investigated

138 area close the Capo D'Orlando Fault. It remains unclear whether or not the 1613 A.D. Naso
139 earthquake (Mw 5.6, Figure 1) ruptured the Capo D'Orlando Fault or other smaller active faults in its
140 surrounding area (epicentres have been located within five km from the investigated area). Towns
141 such as Naso, Capo D'Orlando and Santa Agata di Militello were shaken by a maximum intensity of
142 IX [Guidoboni *et al.*, 2007], indicating a source fault within a few tens of kilometres or less. A second
143 seismic event, the 1739 A.D. Naso earthquake (Mw 5.1), may also have ruptured Capo d'Orlando
144 Fault or other active faults nearby, because maximum intensities of VIII-IX were recorded
145 [Guidoboni *et al.*, 2007]. Empirically-derived structural parameters such as fault length and expected
146 earthquake magnitude [Wells and Coppersmith, 1994; Galli *et al.*, 2008] can be used to suggest that
147 the ~15 km mapped length of the Capo D'Orlando Fault could be capable of producing earthquakes as
148 large as Mw 6, but because the fault length is poorly constrained where it goes offshore in the east,
149 larger magnitudes are not excluded. However, this potential seismogenic structure has not been
150 mapped within the DISS [Basili *et al.*, 2008; INGV - DISS Working Group, 2015] although it shows
151 very similar geological/structural parameters to other mapped "debated seismogenic sources" such as
152 the Vibo Valentia Fault and the Taormina Fault which have themselves been mapped through study of
153 Quaternary deformed palaeoshorelines [Catalano and De Guidi, 2003; De Guidi *et al.*, 2003;
154 Tortorici *et al.*, 2003; Bianca *et al.*, 2011; Roberts *et al.*, 2013]. We note that the Capo D'Orlando
155 Fault may be capable of hosting surface ruptures to earthquakes, because Giunta *et al.* [2012] report
156 kinematic measurements from a striated fault scarp at outcrop, showing dip slip normal movement
157 (see their inset in their Figure 2), implying slip at the surface rather than activity on a blind fault.

158

159 2.2. Late Quaternary palaeoshorelines and existing age controls in the Capo D'Orlando area

160

161 The Calabrian Arc has been experiencing uplift above the Ionian subduction zone suggested
162 by the presence of uplifted Quaternary palaeoshorelines and Holocene coastal notches [Dumas *et al.*,
163 1988, 1993, 2005; Patacca *et al.*, 1990; Westaway, 1993; Miyauchi *et al.*, 1994; Balescu *et al.*, 1997;
164 Stewart *et al.*, 1997; Gvirtzman and Nur, 1999; Bonardi *et al.*, 2001; Doglioni *et al.*, 2001; Faccenna
165 *et al.*, 2004; Lucente *et al.*, 2006; Cucci *et al.*, 2006; Ferranti *et al.*, 2007; Bianca *et al.*, 2011; Roberts

166 *et al.*, 2013] (Figure 1). Furthermore, as already observed by several geoscientists [*Dumas et al.*,
167 1981, 1988, *Ghisetti*, 1981, 1984; *Valensise and Pantosti*, 1992; *Westaway*, 1993; *Miyauchi et al.*,
168 1994; *Bianca et al.*, 1999, 2011; *Catalano and De Guidi*, 2003; *Tortorici et al.*, 2003] the Calabrian
169 Arc provides excellent geological signatures of the interaction between tectonic uplift process and
170 sea-level changes over the Quaternary identified by the presence of dramatic sequences of marine
171 terraces. Here we focus on the fact that tectonically-deformed flights of palaeoshorelines have
172 recorded the effects of Late Quaternary normal faulting activity within the Calabrian Arc [*Jacques et*
173 *al.*, 2001; *Roberts et al.*, 2013]. In agreement with previous authors [e.g. *Armijo et al.*, 1996; *Bianca*
174 *et al.*, 2011; *Giunta et al.*, 2012; *Roberts et al.*, 2013] we interpret mapped seaward-sloping marine
175 surfaces as palaeoshoreface surfaces cut by wave-action, with palaeoshorelines at their up-dip, inner
176 edges, which can be traced parallel to the present-day coastline between the towns of Capo D'Orlando
177 and Acquedolci (Figure 2a and 2b). These palaeoshoreface surfaces have been carved into the "Ghiaie
178 di Messina" Formation and, in places, the Mesozoic limestones and/or the Palaeozoic basement
179 (Figure 3). Furthermore, field observations show that in places these palaeosurfaces have been
180 covered by palaeoshoreface deposits such as sandstones and marine conglomerates (Figure 4). In
181 places, we found rounded, marine beach cobbles made of Mesozoic limestone or Palaeozoic
182 crystalline basement as well as borings made by lithophagids affecting the Mesozoic limestones
183 confirming the geological observations of previous authors [*Scicchitano et al.*, 2011; *Giunta et al.*,
184 2012]. It has been suggested that the Capo D'Orlando Fault has been deforming a partially-dated Late
185 Quaternary sequence of marine terraces in part accommodating the regional extension [*Serpelloni et*
186 *al.*, 2005; *Mastrolembo Ventura et al.*, 2014; *Scarfi et al.*, 2016b; *Chiarabba and Palano*, 2017], and
187 we investigate this further herein.

188 Age control on the marine terrace sequence is limited (Table 1), and here we review existing
189 constraints. *Giunta et al.* [2012] used Optically Stimulated Luminescence (OSL) dating of two
190 samples of marine sands associated with two different palaeoshorelines (their II and IV). The more
191 robust of these is sample 23 on palaeoshoreline II, at an elevation of c. 50 m, near the SW fault tip
192 area between Torrenova and Sant'Agata di Militello town (Figure 2a and 2b). This sample shows
193 robust luminescence behaviour, using a widely-applied protocol, and gives an age of 118 ± 7 ka

194 [Giunta *et al.*, 2012], probably indicating the presence of the ~125 ka palaeoshoreline. An *in-situ* shell
195 of *Spondylus* sp. from sediments just above the marine deposit overlying palaeoshoreline II in the
196 Rocca Scodoni' area was dated by U/Th to c. 125 ka [Scicchitano *et al.*, 2011; Sulli *et al.*, 2013],
197 consistent with the OSL determination. This sequence is located in the hangingwall, close to the
198 centre of the fault if it continues offshore. A further OSL age of 283 ± 22 ka is available from
199 palaeoshoreline IV at 208 m beyond the mapped fault tip close to Fiorita-Sprazzi town (sample 21 in
200 Giunta *et al.* [2012], Figure 2a and 2b). The luminescence characteristics of this sample are not
201 described, but large error bars suggest that the analysis may be close to saturation. Further information
202 would be required to assess the robustness of this age. Other studies have examined a mammal
203 assemblage from deposits at a similar altitude (135 m) to palaeoshoreline III thought to be c. 200 ka
204 old based on isoleucine epimerization dating of bones [Bada *et al.*, 1991]. In this study, we do not use
205 this data point because the stratigraphic link to the marine terrace sequence is tenuous and the method
206 is considered to give relative ages only, despite the attempted quantification.

207 This paucity of absolute age control for mapped palaeoshorelines near Capo D'Orlando is a
208 typical problem for areas affected by low-uplift rates. Thus, a common problem is how to extrapolate
209 the knowledge of known palaeoshoreline ages to help identify the ages of other un-dated
210 palaeoshorelines. Several authors [e.g. Bianca *et al.*, 1999; Catalano *et al.*, 2003; Tortorici *et al.*,
211 2003; Giunta *et al.*, 2012; Gallen *et al.*, 2014] have derived uplift rates by applying a sequential
212 correlation approach. This method is based on the idea that, given a dated palaeoshoreline/horizon, the
213 next higher and older palaeoshoreline is likely to belong to the next older sea-level highstand [e.g.
214 Tortorici *et al.*, 2003; Giunta *et al.*, 2012; Gallen *et al.*, 2014]. However, this method can be prone to
215 error if it does not take into account the well-known "overprinting or re-occupation problem" where
216 palaeo-sea-level highstands that have maximum elevations beneath that of subsequent highstands can
217 be overwhelmed by a subsequent, higher palaeo-sea-level highstand; palaeoshoreline indicators from
218 the former can be eroded and not preserved [Westaway, 1993; Roberts *et al.*, 2013]. If not considered,
219 the overprinting problem can lead to an erroneous assignment of age. Overprinting is particularly
220 problematic in areas with relatively low uplift rates such as southern Italy [Westaway, 1993; Tortorici
221 *et al.*, 2003; Bianca *et al.*, 2011; Giunta *et al.*, 2012; Roberts *et al.*, 2013]. However, Houghton *et al.*

222 [2003] and *Roberts et al.* [2009, 2013] have suggested an alternative approach, whereby an iterative
223 method is used to calculate all expected palaeoshoreline elevations for a given uplift rate, with all
224 measured palaeoshoreline elevations correlated with all predicted palaeoshoreline elevations
225 synchronously rather than sequentially. An example of this approach was demonstrated using the
226 Vibo Fault, Calabria [*Roberts et al.*, 2013]. Here the 125ka-dated palaeoshoreline was used by
227 previous authors [*Tortorici et al.*, 2003; *Bianca et al.*, 2011] to suggest that the next higher
228 palaeoshoreline belonged to the next older major highstand on the sea-level curve (200 ka), thus
229 deriving a temporally-varying uplift rate. However, *Roberts et al.* [2013] verified the age of the
230 125ka-dated palaeoshoreline using $^{238}\text{U}/^{230}\text{Th}$ of corals that formed part of the terrace, and with this
231 age constraint and application of the synchronous correlation method, they showed that the next
232 higher palaeoshoreline was, instead, the 240 ka marine highstand, resulting in a constant uplift rate
233 throughout the Late Quaternary of 0.75 mm/yr (for detailed reference, see Profile 8 in Figure 2a and
234 table 3 in *Roberts et al.* 2013). This approach takes into account the overprinting problem and is
235 considered here to provide more robust estimates of the uplift history than the sequential approach.

236

237 **3. Approach and Methods**

238

239 The study area offers a set of special circumstances that allows investigation of the
240 relationship between regional uplift process and counteracting local tectonics. For example, (i) the
241 Capo D'Orlando normal fault is quasi-parallel to the present-day shoreline, oriented NE–SW, with its
242 displacement decreasing towards the south-west where its tip lies onshore, (ii) hangingwall tectonic
243 subsidence due to normal faulting appears to be slower than the regional uplift process allowing a
244 sequence of marine terraces to be preserved in the hangingwall of the fault, and (iii) the inner edges of
245 the uplifted marine deposits (the palaeoshorelines) can be mapped quasi-parallel to the present-day
246 shoreline. These special circumstances led us to map palaeoshorelines through a detailed DEM-based
247 topographic survey and fieldwork, using existing detailed mapping by *Giunta et al.* [2012] as a guide.
248 We then used a synchronous correlation approach to assign ages to multiple palaeoshorelines, using

249 dating constraints from previous papers [*Scicchitano et al.*, 2011; *Giunta et al.*, 2012]. We also
250 present previous authors dating for the investigated area (Table 1).

251

252 *3.1 Palaeoshoreline elevation data: DEM-based topographic analysis and fieldwork*

253

254 To ensure that we mapped inner edges of marine terraces (palaeoshorelines) which represent
255 the palaeo-sea level related to a highstand, we rely on (i) the presence of key evidence such as
256 lithophagid borings, backshore/foreshore marine deposits containing shallower marine fossils (corals,
257 molluscs, vermetid shells, etc.) as suggested by previous geoscientists [*Ferranti et al.*, 2006; *Roberts*
258 *et al.*, 2009, 2013; *Giunta et al.*, 2012], and (ii) geomorphic features such as coastal notches [*Boulton*
259 *and Stewart*, 2015]. In places, the inner edges of marine terraces can be covered by a few meters of
260 younger terrigenous deposits that produce uncertainty regarding the exact palaeoshoreline elevation.
261 However, our mapping shows these are small in vertical extent (a few metres) and hence the
262 uncertainty is likely to have a minimal impact when calculating the implied uplift rates. Inner-edge
263 elevations defining palaeoshorelines for the Capo D'Orlando area were mapped onto a 10-m
264 resolution Digital Elevation Model (DEM) [*Tarquini et al.*, 2007, 2012] and combined, following
265 ground-truthing during fieldwork, with those published by *Giunta et al.* [2012] (Figure 2a). Fifteen
266 topographic profiles, each capturing a sequence of palaeoshorelines, were produced perpendicular to
267 the strike of the fault covering the 15-km extent of the onshore fault (Figure 2b). The topography and
268 presence of preserved palaeoshoreline indicators was used to decide the location of each
269 palaeoshoreline profile; areas of incision caused by rivers were avoided to ensure that the geomorphic
270 features investigated were marine and not fluvial. The presence of palaeoshorelines was confirmed by
271 extensive geological fieldwork during 2015, with elevations determined using a barometric altimeter
272 that we calibrated to elevation benchmarks such as sea-level every few hours. Note that in places we
273 were unable access the palaeoshorelines locations because of thick vegetation and limited access onto
274 private land. However, analysis of DEMs allowed us to map along strike from our field observations
275 and identify palaeoshoreface surface from slightly seaward-sloping surfaces, bounded up-dip by
276 abrupt palaeocliff-like features marking the palaeoshorelines.

277

278 3.2 Synchronous correlation approach

279

280 The synchronous correlation approach is based on the concept that sea-level highstands,
281 which are thought to produce palaeoshorelines, are unevenly spaced in time, and so for a constant
282 uplift rate, one would expect the palaeoshorelines to be unevenly spaced in elevation. For
283 synchronous correlation, given that at least one palaeoshoreline has age control, the first step is to
284 assume a constant uplift rate and examine whether the implied elevations of palaeoshorelines of
285 different ages match the elevations of measured palaeoshorelines. If they do not, then the uplift-rate
286 can be varied through time and iterated to find the best match with measured palaeoshoreline
287 elevations. This approach was described in detail in *Houghton et al.* [2003] and *Roberts et al.* [2009,
288 2013].

289 To implement the synchronous correlation approach, the method is that topographic profiles
290 are constructed across the strike of the palaeoshorelines from DEM data (Figure 5). Then, using
291 fieldwork to ground-truth the profile, interpretations are made of the inner-edge elevations of
292 palaeoshorelines. These elevations are then input into a spreadsheet that is referred to as the Terrace
293 Calculator [*Roberts et al.*, 2009, 2013]. The initial uplift rate for each profile is constrained using one
294 or more dated palaeoshorelines, which is then used to predict the expected elevations for
295 palaeoshoreline of different ages for comparison with measured elevations. R^2 linear regression
296 analysis quantifies the relationship between the predicted and measured inner-edge elevations. The
297 uplift value is iterated to maximise the R^2 value, with values commonly achieved of > 0.99 . Where
298 there is no dated surface within a profile, the uplift rates of profiles on either side of the one in
299 question are used to determine the initial uplift value and this was then iterated as described above.
300 Once ages are allocated to all of the palaeoshorelines within the sequence of profiles, a comparison of
301 palaeoshoreline elevations versus age parallel to the strike of the fault is used to determine the extent
302 of the along-strike deformation caused by the fault.

303

304 3.3 *Footwall palaeoshorelines and long-term uplift/subsidence ratio to derive throw-rate on*
305 *Capo D'Orlando Fault*

306

307 Palaeoshorelines have been mapped both on the hangingwall and partially on the footwall of
308 the Capo D'Orlando Fault (see Topographic profile 7, Fig. 6). In particular, a wave cut platform
309 (WCP) cut into limestone associated with Late Quaternary palaeoshoreline deposits has been mapped
310 on its footwall close to the supposed centre of the onshore fault segment at 345 m above sea level
311 (a.s.l) (Figure 2b). Evidence of an upper shoreface marine environment have been recognized such as
312 rounded marine beach cobbles, possible mill-holes and poorly-preserved and hence equivocal
313 lithophagid borings, all of which probably indicate a palaeo-rocky beach. We use the elevations of
314 these footwall wave cut platforms, and their hangingwall equivalents identified mapping around the
315 SW fault tip, to estimate long-term fault displacement by applying a long-term uplift/subsidence ratio
316 proposed by several authors [*King et al.*, 1988; *Armijo et al.*, 1996; *McNeill and Collier*, 2004]. A
317 value of 1/3.5 (uplift/subsidence) ratio has been applied, and we use the elevation of the 340 ka
318 palaeoshoreline mapped close the centre of fault on the hangingwall at 129 m and within the fault “tip
319 zone” at 291 m as being the correlative surface with the lowest WCP on the footwall.

320

321 **4. Results**

322 First, we show that the approach advocated above can re-produce measured palaeoshoreline
323 elevations by matching them with predicted elevations. We then correlate palaeoshoreline elevations
324 along-strike for the Capo D'Orlando Fault. Finally, we use the derived spatial and temporal
325 constraints on the palaeoshoreline geometries to derive uplift rates and how these relate to
326 displacements on the active normal fault.

327 We show our synchronous correlation between mapped palaeoshorelines and palaeoshore
328 elevations predicted through iteration of the uplift rate (Figure 6). We iterated the uplift rates to find
329 the best fit between mapped and predicted palaeoshorelines using the dual criteria of (i) making sure
330 that the clearest mapped palaeoshorelines were matched by the most prominent sea-level highstands at
331 125, 240 and 340 ka, and (ii) maximising the R^2 value that shows how well other less prominent

332 mapped palaeoshorelines match the predicted palaeoshoreline elevations. Through our synchronous
333 correlation we are able to reassess ages for all mapped but un-dated palaeoshorelines (Table 2). It is
334 important to note that our interpreted palaeo-sea-cliffs defining palaeoshorelines are clear on the
335 DEM. However, in places some of the palaeoshorelines are too small in geographic extent to see at
336 the resolution of the DEM, yet were clear during the fieldwork (Figure 4 for the Profile 6 with
337 the 125ka-dated palaeoshoreline clear in the field). Nonetheless, we have indicated these subtle
338 mapped palaeoshorelines and included them in the synchronous correlation (Figure 6). In order to
339 check (a) the correlation between elevations determined from the DEM and those measured with a
340 hand-held barometric altimeter in the field, and (b) how well the measured elevations match the
341 predicted elevations from synchronous correlation (Figure 7). We find that (a) elevations measured on
342 the DEM match those measured in the field within measurement error, suggesting our measured
343 elevations are robust (Figure 7a), and (b) our predicted elevations match the measured ones within
344 error, suggesting we have gained a robust correlation, and reliable uplift-rate estimates (Figure 7b).

345 The linear regression analysis described above implies a robust, synchronous correlation
346 between multiple sea-level highstands and multiple palaeoshoreline elevations. This key observation
347 also suggests that uplift rates have not fluctuated through time. Another implication is that we have
348 identified palaeoshorelines associated with the sea-level highstands from 76 ka, 100 ka, 125 ka, 175
349 ka, 200 ka, 217 ka, 240 ka, 285 ka, 310 ka, 340 ka and 410 ka (not all mapped within a single profile)
350 (Table 3); these synchronously-derived ages of palaeoshorelines have been recognised elsewhere in
351 the Mediterranean area [e.g. *Roberts et al.*, 2009, 2013]. Our results also confirm that mapping by
352 *Giunta et al.* [2012] is reliable and robust, but we assign amended ages to his mapped
353 palaeoshorelines.

354 We use our interpretations between multiple mapped palaeoshorelines and multiple
355 iteratively-predicted highstand elevations to produce a correlation of palaeoshorelines along the strike
356 of the Capo D'Orlando Fault (Figure 8). In particular, our synchronous correlation shows that uplift
357 rates are constant over the Late Quaternary yet vary spatially, with an uplift rate of 0.35 mm/yr in the
358 centre of the hangingwall of the fault, increasing towards the fault tip and beyond where the uplift rate
359 is 0.89 mm/yr (Figure 8a). Because the uplifted palaeoshorelines are in the hangingwall of the Capo

360 D'Orlando Fault, this suggests that finite uplift is a combination of a "regional" uplift signal and local
361 fault-controlled subsidence.

362 The observation that uplift varies along the strike of the fault, with folded and tilted
363 palaeoshorelines (Figure 8b), suggests that there is a displacement gradient along the fault. We have
364 investigated whether folding and tilting have occurred through time or after formation of all the
365 palaeoshorelines by examining values of tilt along strike and how these vary for different
366 palaeoshoreline ages. If faulting has occurred progressively through time we would expect older
367 palaeoshorelines to be more tilted than younger ones along the strike of the fault. Note that tilt angle
368 values for each investigated palaeoshoreline have been calculated, as a \tan^{-1} of a gradient "m" of
369 straight line equation ($y=mx$). We then show that older and higher mapped palaeoshorelines present
370 higher tilt angle values, implying that they have experienced a longer history of faulting activity
371 (Figure 8c). We interpret this evidence to indicate that faulting has occurred progressively through
372 time, during the progressive formation of successive palaeoshorelines. Our interpretations also reveal
373 another stratigraphic feature consistent with along-strike variation in fault activity rate. The implied
374 increase in uplift rate in the hangingwall of the fault towards the fault tip has allowed more
375 palaeoshorelines to be preserved where the uplift rate is higher (Figure 8b). This fact is to be expected
376 because the overprinting problem mentioned above will destroy some palaeoshorelines if the uplift
377 rate is low. Thus, the increase in the number of palaeoshorelines with uplift rate and increase in tilt
378 angle with age are both diagnostic of incremental fault-controlled deformation, and similar features
379 have been reported for other areas deformed by active normal faults in the Gulf of Corinth [*Armijo et*
380 *al.*, 1996; *Roberts et al.*, 2009] and the Calabrian Arc [*Roberts et al.*, 2013].

381 We recognize a "tip zone" defined by (i) higher number of preserved marine terraces, (ii) a
382 shallowing of the long-term tilt angle value recorded by palaeoshorelines from NE to SW and (iii)
383 field-based evidence showing that the fault scarp mapped by Giunta et al. [2012] dies out along strike
384 towards the tip zone (Figure 8b). This "zone" in figure 2b coincides with the red-coloured dashed line
385 in the SW fault tip. This observation provides the opportunity to attempt to correlate hangingwall
386 palaeoshorelines with those on the footwall by mapping them around the fault tip. It, in turn, allows us
387 to calculate the throw-rate on the fault. Our field mapping suggests a correlation between the

388 hangingwall palaeoshoreline that (i) we have assigned to the 340 ka sea-level highstand, and (ii) we
389 have mapped at 291 m in the tip zone, with a footwall palaeoshoreline that we have mapped to the NE
390 in the footwall at an elevation of 345 m near the middle of the footwall of the fault. In other words, we
391 have been able to correlate a palaeoshoreline across the fault from the hangingwall to the footwall. To
392 gain the rate of vertical offset we have (i) applied a long-term uplift/subsidence ration of 1/3.5 along
393 Profile 7 at the centre of fault, intercepting the WCP mapped in the footwall to predict the footwall
394 elevation of the 340 ka palaeoshoreline, and (ii) taken into account the implied “minimum
395 displacement” (or the hangingwall subsidence) for the 340 ka palaeoshoreline calculated between the
396 hangingwall elevation and the elevation within the fault tip zone (Profile 13). We obtained a
397 “predicted” footwall palaeoshoreline elevation of 335 m which we suggest could be associated with
398 the 345 m high palaeoshoreline that we have mapped in the footwall. The offset between the footwall
399 and the hangingwall implies a constant long-term fault throw-rate of 0.63 ± 0.02 mm/yr derived by a
400 fault throw of 216 m for the last 340 kyrs (Figure 8b). Note that the uncertainty has been estimated by
401 applying a formula to calculate error propagation as follows: $dTR = |TR| \cdot \sqrt{[(dD/D)^2 + (dt/T)^2]}$
402 where dTR is the calculated uncertainty, TR (0.63 mm/yr) is the throw rate, D (216 m = 216000 mm)
403 is the measured displacement and T (340 kyr = 340000 yr) is the time over the displacement occurred.
404 Furthermore, error value associated with the displacement (dD) is 5000 mm which is derived by
405 barometric altimeter error resolution; error value associated with the age of highstand (dT) is 4000 yr
406 [Siddall *et al.*, 2003; Rohling *et al.*, 2014].

407 These results confirm that the Capo D’Orlando Fault has been offsetting the investigated
408 palaeoshorelines at the surface throughout the Late Quaternary, proving that this fault is not blind.
409 Our interpretations described above suggest that the regional uplift can be defined within and beyond
410 the tip-zone of the Capo D’Orlando Fault; it is implied that this value is ~ 0.9 mm/yr. However, note
411 that further detailed studies are needed to define whether this candidate value for the regional uplift is
412 in fact influenced by possible active faults offshore.

413

414 **5. Discussion**

415

416 In this study, we have investigated the relationship between multiple Late Quaternary
417 palaeoshorelines, active normal faulting and regional uplift. Our results indicate a long-term constant
418 fault throw-rate and related fault-modified regional uplift rate, rather than an uplift rate that fluctuates
419 through time (Figure 9). Recognition that the Capo D’Orlando Fault has modified the “regional” uplift
420 signal with a constant rate has implications for the geography of the seismic hazard of NE Sicily and
421 within the wider area of the geological domain of the Calabrian Arc (Figure 10). In particular, it
422 implies that slip distributions calculated for subduction interfaces based on uplift data need to
423 consider ongoing crustal deformation within the upper plate. We discuss this in more detail with
424 regard to local and regional processes.

425

426 *5.1. Local tectonic implications: estimating fault throw-rate and Earthquake Recurrence*
427 *Interval for the Capo D’Orlando Fault*

428

429 At the local scale, the investigated area shows clear evidence that the uplift rate field varies
430 along strike of the Capo D’Orlando Fault (Figure 8a), indicating that this normal fault is active. This
431 fact is not surprising considering that NE Sicily has been affected by historical damaging earthquakes
432 (Figure 1). Therefore, we suggest that the Capo D’Orlando Fault should be added within DISS at least
433 as “Debated Seismogenic Source” to improve the seismic hazard assessment for the NE Sicily.

434 For the Capo D’Orlando Fault, we suggest a constant throw-rate of 0.63 ± 0.02 mm/yr on the
435 as the most likely scenario by investigating fault-deformed Late Quaternary palaeoshorelines
436 outcropping in the hangingwall and footwall of this fault (Figure 9). The throw-rate value is not
437 unusual considering that slip-rate values measured for other active normal faults which have been
438 accommodating the Plio-Pleistocene crustal extension along the Italian Apennines and the Calabrian
439 Arc are within the range 0.3 mm/yr to 2.0 mm/yr [Jacques *et al.*, 2001; Galli and Bosi, 2002; Roberts
440 and Michetti, 2004]. Also, well-known empirical correlations between fault length, maximum
441 expected magnitude and maximum expected displacement [Wells and Coppersmith, 1994; Galli *et al.*,
442 2008] allow us to calculate, for the first time, an estimated earthquake recurrence interval or T_{mean} for
443 the Capo D’Orlando Fault which, considering the length of the fault mapped onshore, could be

444 capable of earthquakes with maximum magnitude (M) of 6.2. To produce a fault throw-rate of $0.63 \pm$
445 0.02 mm/yr given 50 cm maximum vertical slip events in Mw 6.2 earthquakes implies an earthquake
446 recurrence interval of 820 years; this value is comparable to those that characterize active normal
447 faults along the Italian peninsula [Jacques *et al.*, 2001; Galli *et al.*, 2008; Roberts *et al.*, 2013].
448 However, the NE tip of the fault has not identified because hangingwall uplift (that is hangingwall
449 subsidence plus regional uplift) is still low relative to the tip zone that has been identified at the SW
450 end of the fault (Figure 8). We suggest that the NE fault tip is likely to be offshore, implying a longer
451 fault length. If the Capo D'Orlando Fault is longer than 15 km, this increases the possible maximum
452 earthquake magnitude to $> Mw 6.2$; in turn, it implies larger slip events and hence longer earthquake
453 recurrence intervals, suggesting that further study of the offshore are needed. We point out that we
454 have explored a scenario using a possible maximum magnitude earthquake, assuming that earthquakes
455 rupture along the entire length of the Capo D'Orlando Fault; shorter recurrence intervals are implied if
456 only part of the fault length ruptures.

457

458 *5.2. Crustal deformation within the upper plate of the Ionian subduction zone: regional*
459 *tectonic implications, slip distribution calculations, mantle-related uplift and the associated seismic*
460 *hazard on subduction zones*

461

462 Our study shows that the “regional” uplift signal, within the upper plate of the Ionian
463 subduction zone since the Late Quaternary, has been spatially perturbed by “local” crustal
464 deformation that needs to be considered to attempt long-term seismic hazard assessment.

465 Generally, it is common to infer slip distributions on the subduction interface and mantle
466 upwelling processes from observations of uplift in the upper plate of the subduction zone [e.g.
467 Gvirtzman and Nur, 1999; Wortel and Spakman 2000; D'Agostino *et al.*, 2001; McCloskey *et al.*,
468 2005; Meltzner *et al.*, 2006; Faure Walker *et al.*, 2012; Nalbant *et al.*, 2013; Nic Bhloscaidh *et al.*,
469 2015]. The Ionian subduction associated with roll-back of the Ionian slab [Goes *et al.*, 2004], and
470 asthenospheric upwelling beneath the continental crust of the Calabrian Arc [Gvirtzman and Nur,

1999; *Wortel and Spakman, 2000*] has occurred synchronously with uplift of the Calabrian forearc over the Late Quaternary. However, we emphasise that the Calabrian Arc shows prominent intra-crustal deformation mostly in the form of active normal faulting controlling the topography of the area (Figure 10). In particular, topographic highs exist due to tectonic uplift in the footwalls of active normal faults such as the Maratea Fault [e.g. *Papanikolaou and Roberts, 2007*], the Pollino Fault [e.g. *Michetti et al., 1997*], the Vibo Fault [e.g. *Roberts et al., 2013*], the Cittanova Fault [e.g. *Jacques et al., 2001; Galli and Bosi, 2002; Roda-Boluda and Whittaker, 2017*], the Taormina Fault [e.g. *Catalano and De Guidi, 2003; De Guidi et al., 2003; Spampinato et al., 2012*] and the Capo D'Orlando Fault itself [e.g. *Scicchitano et al., 2011; Giunta et al., 2012* and this study] (Figure 1). These faults have been seismically deforming the upper plate of the Ionian subduction zone producing damaging earthquakes. Spatial variation in uplift rates measured over (i) the Late Quaternary [*Antonioli et al., 2006, 2009; Ferranti et al., 2006; Roberts et al., 2013* and this study] and (ii) the last decades shown by using GPS analysis [*Serpelloni et al., 2013*] along the strike of these faults (Figure 10a and 10b) imply that uplift is not simply controlled either by slip on the subduction interfaces or mantle upwelling-related dynamic topography; the upper plate seismogenic sources will strongly affect the “regional” uplift over wavelengths of a few tens of kilometres within the Calabrian Arc, implying that these normal faults need to be well-defined. We suggest that differential uplift due to the “local effect” of normal faulting has been occurring through time along the Calabrian forearc (Figure 8 and 9). Therefore, if the variation in uplift rates due to these normal faults is not recognised and removed from calculations, this could lead to (i) overly complicated and misleading subduction interface slip distributions and (ii) erroneous conclusions about the dynamic topography, due to the mantle upwelling [*D'Agostino et al., 2001; Faure Walker et al., 2012*]. We emphasise that such upper plate normal faulting is widespread with clear examples in central Greece and Crete, Japan and south America [*Armijo et al., 1996; Hasegawa et al., 2000; Saillard et al., 2011; Vacchi et al., 2012; Gallen et al., 2014; Binnie et al., 2016*]. One finding that is now emerging is that for at least some upper plate normal faults, the throw-rate on the fault through the Late Quaternary is constant through time (e.g. 0.63 ± 0.02 mm/yr from this study), rather than fluctuating through time [e.g. *Giunta et al., 2012*] (Figure 9). For example, a constant throw-rate through the late Quaternary has also been reported for

499 the Vibo Fault, within the Calabrian Arc [Roberts *et al.* 2013]. If this is common it is implied that
500 constant values of uplift through time need to be subtracted from regional uplift-rate signals if
501 subduction zone slip distributions and mantle dynamics are to be inferred.

502 Turning to the regional contribution of the Capo D'Orlando Fault to the regional extension,
503 we suggest that in order to accommodate geodetically-derived regional extension rates of ~ 2 mm/yr
504 [Serpelloni *et al.*, 2005] or ~ 3 mm/yr [Mastrolembo Ventura *et al.*, 2014] a well-constrained long-
505 term constant throw-rate through time on the Capo D'Orlando Fault of 0.63 ± 0.02 mm/yr implies that
506 additional crustal deformation has to be accommodated by other active faults across strike. It also
507 perhaps implies that faults across strike will also need to remain active through time to maintain
508 constant throw-rates and hence slip-rates [e.g. Roberts *et al.*, 2002]. Seismic profiles quasi-
509 perpendicular to the coastline of Capo D'Orlando area have already shown offshore crustal
510 extensional processes due to normal faulting [Nigro and Sulli, 1995]. It would be interesting to see
511 whether these faults also have constant slip-rates.

512 However, note that in other locations, active fault systems have been shown to be
513 accommodating crustal deformation with associated rates varying through time. For instance,
514 tectonically-deformed uplifted marine terraces have been investigated within the Gulf of Corinth in
515 Greece [Roberts *et al.*, 2009] who suggest varying long-term fault slip-rates, implying a synchronous
516 change in faulting activity on active faults across strike. In particular, the investigated South
517 Alkyonides active fault in the Gulf of Corinth, Greece, has accelerated its slip-rate synchronous with a
518 deceleration on other faults located across strike over the Late Quaternary [Roberts *et al.*, 2009]. This
519 evidence suggests that when active faults are arranged across strike and interacting, activity can swap
520 back and forth through time on a multi-millennium timescale to accommodate the regional deformation
521 [Roberts *et al.*, 2002; Bennett *et al.*, 2004; Cowie *et al.*, 2005; Dolan *et al.*, 2007; Nixon *et al.*, 2016].
522 We stress that more studies are needed to better identify the locations long-term crustal deformation,
523 and how they change through time, by studying (i) sequences of tectonically-deformed Late
524 Quaternary marine terraces onshore and (ii) seismic profiles to define faulting activity offshore the
525 investigated area.

526 Overall, we suggest that local deformation rates measured over the Late Quaternary on upper
527 plate normal faults provide important insights into the subduction process. The deformation within the
528 upper plate must be subtracted to derive a better understanding of subduction and mantle upwelling,
529 and allow calculation of more robust slip distributions for subduction interface events to feed into
530 seismic hazard analysis associated with subduction-related earthquakes. This knowledge help to
531 understand the seismic hazard related to the upper plate of the Ionian subduction zone in southern
532 Italy.

533

534 **6. Conclusion**

535

536 In this paper, we report constant crustal deformation rates through time on a normal fault
537 within the upper plate of the Ionian subduction zone. Late Quaternary palaeoshorelines deformed by
538 the Capo D'Orlando Fault have been investigated by applying a synchronous correlations method.
539 The study shows that the Capo D'Orlando Fault is an active and potential seismic source with a
540 throw-rate of 0.63 ± 0.02 mm/yr that has been constant through the late Quaternary. In particular, we
541 show that fault displacements have folded and tilted the investigated palaeoshorelines along the strike
542 of the fault, and that higher and older palaeoshorelines have experienced a longer faulting history. The
543 deformed palaeoshorelines demonstrate that the Capo D'Orlando fault is active and should be
544 included in seismic hazard assessments of NE Sicily. The throw-rate of 0.63 ± 0.02 mm/yr has been
545 constant through time showing that other unidentified active faults are needed to explain the observed
546 2-3 mm/yr of regional extension measured with GPS. The results suggest that care is needed to
547 include or exclude upper plate deformation, using surface uplift data, when inferring (i) mantle
548 upwelling-related dynamic topography and (ii) slip distributions on subduction interfaces.

549

550 **Acknowledgements**

551 This work was funded and supported by the London NERC DTP Scholarship (grant number
552 reference: 1492238). We thank the editor Taylor Schildgen, the associate editor, Sarah Boulton,
553 Joshua Spinler and an anonymous reviewer for the insightful comments which allowed to improve the

554 paper. We thank Simone Tarquini for helping us to access the DEMs (TINITALY). Gianfranco
555 Scicchitano and Fabrizio Antonioli are thanked for their helpful discussions on the dated location
556 along Profile 6. Francesco Pio Lucente is thanked for providing us Figure 1c.
557 All data for this paper are properly cited and referred to in the reference list and available on Figure 6
558 as topographic data where palaeoshoreline elevations have been mapped and in Table 2. These data
559 can be used to re-produce Results shown in Figure 7, 8 and 9. They are also available by contacting
560 the corresponding author (marco.meschis.14@ucl.ac.uk or marco.meschis@gmail.com).

561

562 **References**

- 563 Antonioli, F., S. Kershaw, P. Renda, D. Rust, G. Belluomini, M. Cerasoli, U. Radtke, and S. Silenzi
564 (2006a), Elevation of the last interglacial highstand in Sicily (Italy): A benchmark of coastal
565 tectonics, *Quat. Int.*, 145–146, 3–18, doi:10.1016/j.quaint.2005.07.002.
- 566 Antonioli, F., L. Ferranti, K. Lambeck, S. Kershaw, V. Verrubbi, and G. Dai Pra (2006b), Late
567 Pleistocene to Holocene record of changing uplift rates in southern Calabria and northeastern
568 Sicily (southern Italy, Central Mediterranean Sea), *Tectonophysics*, 422(1–4), 23–40,
569 doi:10.1016/j.tecto.2006.05.003.
- 570 Antonioli, F. et al. (2009), Holocene relative sea-level changes and vertical movements along the
571 Italian and Istrian coastlines, *Quat. Int.*, 206(1–2), 102–133, doi:10.1016/j.quaint.2008.11.008.
- 572 Armijo, R., H. Lyon-Caen, and D. Papanastassiou (1992), East-west extension and Holocene normal-
573 fault scarps in the Hellenic arc, *Geology*, 20(6), 491–494, doi:10.1130/0091-
574 7613(1992)020<0491:EWEAHN>2.3.CO;2.
- 575 Armijo, R., B. Meyer, G. C. P. King, A. Rigo, and D. Papanastassiou (1996), Quaternary evolution of
576 the Corinth Rift and its implications for the Late Cenozoic evolution of the Aegean, *Geophys. J.*
577 *Int.*, 126(1), 11–53, doi:10.1111/j.1365-246X.1996.tb05264.x.
- 578 Bada, J. L., G. Belluomini, L. Bonfiglio, M. Branca, E. Burgio, and L. Delitala (1991), Isoleucine
579 epimerization ages of Quaternary mammals from Sicily, *Quat.*, 4, 49–54.
- 580 Balescu, S., B. Dumas, P. Gu er emy, M. Lamothe, R. Lh enaff, and J. Raffy (1997),
581 Thermoluminescence dating tests of Pleistocene sediments from uplifted marine shorelines

582 along the southwest coastline of the Calabrian Peninsula (southern Italy), *Palaeogeogr.*
583 *Palaeoclimatol. Palaeoecol.*, 130(1–4), 25–41, doi:10.1016/S0031-0182(96)00119-8.

584 Barone, A., A. Fabbri, S. Rossi, and R. Sartori (1982), Geological structure and evolution of the
585 marine areas adjacent to the Calabrian Arc, *Earth Evol. Sci.*, 3, 207–221.

586 Basili, R., G. Valensise, P. Vannoli, P. Burrato, U. Fracassi, S. Mariano, M. M. Tiberti, and E. Boschi
587 (2008), The Database of Individual Seismogenic Sources (DISS), version 3: Summarizing
588 20 years of research on Italy’s earthquake geology, *Tectonophysics*, 453(1–4), 20–43,
589 doi:10.1016/j.tecto.2007.04.014.

590 Bennett, R. A., A. M. Friedrich, and K. P. Furlong (2004), Codependent histories of the San Andreas
591 and San Jacinto fault zones from inversion of fault displacement rates, *Geology*, 32(11), 961,
592 doi:10.1130/G20806.1.

593 Bianca, M., C. Monaco, L. Tortorici, and L. Cernobori (1999), Quaternary normal faulting in
594 southeastern Sicily (Italy): a seismic source for the 1693 large earthquake, *Geophys. J. Int.*,
595 139(2), 370–394, doi:10.1046/j.1365-246x.1999.00942.x.

596 Bianca, M., S. Catalano, G. De Guidi, A. . Gueli, C. Monaco, G. M. Ristuccia, G. Stella, G. Tortorici,
597 L. Tortorici, and S. O. Troja (2011), Luminescence chronology of Pleistocene marine terraces of
598 Capo Vaticano peninsula (Calabria, Southern Italy), *Quat. Int.*, 232(1–2), 114–121,
599 doi:10.1016/j.quaint.2010.07.013.

600 Binnie, A., T. J. Dunai, S. A. Binnie, P. Victor, G. González, and A. Bolten (2016), Accelerated late
601 quaternary uplift revealed by 10 Be exposure dating of marine terraces, Mejillones Peninsula,
602 northern Chile, *Quat. Geochronol.*, 36, 12–27, doi:10.1016/j.quageo.2016.06.005.

603 Bonardi, G., W. Cavazza, V. Perrone, and S. Rossi (2001), Calabria-Peloritani terrane and northern
604 Ionian sea, in *Anatomy of an Orogen: The apennines and adjacent mediterranean basins*, pp.
605 287–306, Springer.

606 Boulton, S. J., and I. S. Stewart (2015), Holocene coastal notches in the Mediterranean region:
607 Indicators of palaeoseismic clustering?, *Geomorphology*, 237, 29–37,
608 doi:10.1016/j.geomorph.2013.11.012.

609 Catalano, S., and G. De Guidi (2003), Late Quaternary uplift of northeastern Sicily: Relation with the

610 active normal faulting deformation, *J. Geodyn.*, 36(4), 445–467, doi:10.1016/S0264-
611 3707(02)00035-2.

612 Catalano, S., G. De Guidi, C. Monaco, G. Tortorici, and L. Tortorici (2003), Long-term behaviour of
613 the late Quaternary normal faults in the Straits of Messina area (Calabrian arc): Structural and
614 morphological constraints, *Quat. Int.*, 101–102(1), 81–91, doi:10.1016/S1040-6182(02)00091-5.

615 Chapman, N., K. Berryman, P. Villamor, W. Epstein, L. Cluff, and H. Kawamura (2014), Active
616 Faults and Nuclear Power Plants, *Eos, Trans. Am. Geophys. Union*, 95(4), 33–34,
617 doi:10.1002/2014EO040001.

618 Chiarabba, C., and M. Palano (2017), Progressive migration of slab break-off along the southern
619 Tyrrhenian plate boundary: Constraints for the present day kinematics, *J. Geodyn.*, 105, 51–61,
620 doi:<https://doi.org/10.1016/j.jog.2017.01.006>.

621 Cowie, P., J. Underhill, M. Behn, J. Lin, and C. Gill (2005), Spatio-temporal evolution of strain
622 accumulation derived from multi-scale observations of Late Jurassic rifting in the northern North
623 Sea: A critical test of models for lithospheric extension, *Earth Planet. Sci. Lett.*, 234(3–4), 401–
624 419, doi:10.1016/j.epsl.2005.01.039.

625 Cowie, P. a., G. P. Roberts, J. M. Bull, and F. Visini (2012), Relationships between fault geometry,
626 slip rate variability and earthquake recurrence in extensional settings, *Geophys. J. Int.*, 189(1),
627 143–160, doi:10.1111/j.1365-246X.2012.05378.x.

628 Cucci, L., A. Tertulliani, I. Nazionale, S. Sismologia, and V. Murata (2006), I Terrazzi Marini Nell '
629 Area Di Capo Vaticano (Arco Calabro): Solo Un Record Di Sollevamento Regionale O Anche
630 Di Deformazione Cosismica ?, *Quat.*, 19(1), 89–101.

631 D'Agostino, N., J. A. Jackson, F. Dramis, and R. Funiciello (2001), Interactions between mantle
632 upwelling, drainage evolution and active normal faulting: an example from the central
633 Apennines (Italy), *Geophys. J. Int.*, 147(2), 475–497, doi:10.1046/j.1365-246X.2001.00539.x.

634 Dewey, J. F., M. L. Helman, S. D. Knott, E. Turco, and D. H. W. Hutton (1989), Kinematics of the
635 western Mediterranean, *Geol. Soc. London, Spec. Publ.*, 45(1), 265–283,
636 doi:10.1144/GSL.SP.1989.045.01.15.

637 Doglioni, C., F. Innocenti, and G. Mariotti (2001), Why Mt Etna ?, *Terra Nov.*, 13, 25–31.

638 Dolan, J. F., D. D. Bowman, and C. G. Sammis (2007), Long-range and long-term fault interactions in
639 Southern California, *Geology*, 35(9), 855–858, doi:10.1130/G23789A.1.

640 Dumas, B., P. Gueremy, R. Lhenaff, and J. Raffy (1981), Le soulèvement quaternaire de la Calabre
641 méridionale, *Rev. Géologie Dyn. Géographie Phys. Paris*, 23, 27–40.

642 Dumas, B., P. Gueremy, P. J. Hearty, R. Lhenaff, and J. Raffy (1988), Morphometric analysis and
643 amino acid geochronology of uplifted shorelines in a tectonic region near Reggio Calabria,
644 South Italy, *Palaeogeogr. Palaeoclimatol. Palaeoecol.*, 68(2–4), 273–289, doi:10.1016/0031-
645 0182(88)90045-4.

646 Dumas, B., P. Gueremy, R. Lhenaff, and J. Raffy (1993), Rapid uplift, stepped marine terraces and
647 raised shorelines on the Calabrian coast of Messina Strait, Italy, *Earth Surf. Process. Landforms*,
648 18(3), 241–256, doi:10.1002/esp.3290180306.

649 Dumas, B., P. Guérémy, and J. Raffy (2005), Evidence for sea-level oscillations by the “characteristic
650 thickness” of marine deposits from raised terraces of Southern Calabria (Italy), *Quat. Sci. Rev.*,
651 24(18–19), 2120–2136, doi:10.1016/j.quascirev.2004.12.011.

652 Faccenna, C., C. Piromallo, A. Crespo-Blanc, L. Jolivet, and F. Rossetti (2004), Lateral slab
653 deformation and the origin of the western Mediterranean arcs, *Tectonics*, 23(1), n/a-n/a,
654 doi:10.1029/2002TC001488.

655 Faccenna, C., P. Molin, B. Orecchio, V. Olivetti, O. Bellier, F. Funiciello, L. Minelli, C. Piromallo,
656 and A. Billi (2011), Topography of the Calabria subduction zone (southern Italy): Clues for the
657 origin of Mt. Etna, *Tectonics*, 30(1), 1–20, doi:10.1029/2010TC002694.

658 Faccenna, C., T. W. Becker, M. S. Miller, E. Serpelloni, and S. D. Willett (2014), Isostasy, dynamic
659 topography, and the elevation of the Apennines of Italy, *Earth Planet. Sci. Lett.*, 407, 163–174,
660 doi:10.1016/j.epsl.2014.09.027.

661 Faure Walker, J. P., G. P. Roberts, P. R. Sammonds, and P. Cowie (2010), Comparison of earthquake
662 strains over 10² and 10⁴ year timescales: Insights into variability in the seismic cycle in the
663 central Apennines, Italy, *J. Geophys. Res.*, 115(B10), B10418, doi:10.1029/2009JB006462.

664 Faure Walker, J. P., G. P. Roberts, P. A. Cowie, I. Papanikolaou, A. M. Michetti, P. Sammonds, M.
665 Wilkinson, K. J. W. McCaffrey, and R. J. Phillips (2012), Relationship between topography,

666 rates of extension and mantle dynamics in the actively-extending Italian Apennines, *Earth*
667 *Planet. Sci. Lett.*, 325–326, 76–84, doi:10.1016/j.epsl.2012.01.028.

668 Ferranti, L. et al. (2006), Markers of the last interglacial sea-level high stand along the coast of Italy:
669 Tectonic implications, *Quat. Int.*, 145–146, 30–54, doi:10.1016/j.quaint.2005.07.009.

670 Ferranti, L., C. Monaco, F. Antonioli, L. Maschio, S. Kershaw, and V. Verrubbi (2007), The
671 contribution of regional uplift and coseismic slip to the vertical crustal motion in the Messina
672 Straits, southern Italy: Evidence from raised Late Holocene shorelines, *J. Geophys. Res.*,
673 112(B6), B06401, doi:10.1029/2006JB004473.

674 Friedrich, A. M., B. P. Wernicke, N. A. Niemi, R. A. Bennett, and J. L. Davis (2003), Comparison of
675 geodetic and geologic data from the Wasatch region, Utah, and implications for the spectral
676 character of Earth deformation at periods of 10 to 10 million years, *J. Geophys. Res. Solid Earth*,
677 108(B4), 2199, doi:10.1029/2001JB000682.

678 Gallen, S. F., K. W. Wegmann, D. R. Bohnenstiehl, F. J. Pazzaglia, M. T. Brandon, and C. Fassoulas
679 (2014), Active simultaneous uplift and margin-normal extension in a forearc high, Crete,
680 Greece, *Earth Planet. Sci. Lett.*, 398, 11–24, doi:10.1016/j.epsl.2014.04.038.

681 Galli, P., and V. Bosi (2002), Paleoseismology along the Cittanova fault: Implications for
682 seismotectonics and earthquake recurrence in Calabria (southern Italy), *J. Geophys. Res.*,
683 107(B3), 2044, doi:10.1029/2001JB000234.

684 Galli, P., F. Galadini, and D. Pantosti (2008), Twenty years of paleoseismology in Italy, *Earth-*
685 *Science Rev.*, 88(1–2), 89–117, doi:10.1016/j.earscirev.2008.01.001.

686 Ghisetti, F. (1981), Upper Pliocene-Pleistocene uplift rates as indicators of neotectonic pattern: an
687 example from southern Calabria (Italy), *Z. Geomorphol*, 40, 93–118.

688 Ghisetti, F. (1984), Recent deformations and the seismogenic source in the Messina Strait (southern
689 Italy), , 109, 191–208, doi:https://doi.org/10.1016/0040-1951(84)90140-9.

690 Ghisetti, F., and L. Vezzani (1982), Different styles of deformation in the calabrian arc (Southern
691 Italy): Implications for a seismotectonic zoning, *Tectonophysics*, 85(3–4), 149–165,
692 doi:10.1016/0040-1951(82)90101-9.

693 Giunta, G., A. M. Gueli, C. Monaco, S. Orioli, G. M. Ristuccia, G. Stella, and S. O. Troja (2012),

694 Middle-Late Pleistocene marine terraces and fault activity in the Sant'Agata di Militello coastal
695 area (north-eastern Sicily), *J. Geodyn.*, 55, 32–40, doi:10.1016/j.jog.2011.11.005.

696 Goes, S., D. Giardini, S. Jenny, C. Hollenstein, H.-G. Kahle, and A. Geiger (2004), A recent tectonic
697 reorganization in the south-central Mediterranean, *Earth Planet. Sci. Lett.*, 226(3–4), 335–345,
698 doi:10.1016/j.epsl.2004.07.038.

699 De Guidi, G., S. Catalano, C. Monaco, and L. Tortorici (2003), Morphological evidence of Holocene
700 coseismic deformation in the Taormina region (NE Sicily), *J. Geodyn.*, 36(1–2), 193–211,
701 doi:10.1016/S0264-3707(03)00047-4.

702 Guidoboni, E., G. Ferrari, D. Mariotti, A. Comastri, G. Tarabusi, and G. Valensise (2007), Catalogue
703 of Strong Earthquakes in Italy (461 BC-1997) and Mediterranean Area (760 BC-1500),

704 Gutscher, M.-A. et al. (2017), Active tectonics of the Calabrian subduction revealed by new multi-
705 beam bathymetric data and high-resolution seismic profiles in the Ionian Sea (Central
706 Mediterranean), *Earth Planet. Sci. Lett.*, 461, 61–72, doi:10.1016/j.epsl.2016.12.020.

707 Gvirtzman, Z., and A. Nur (1999), The formation of Mount Etna as the consequence of slab rollback,
708 *Nature*, 401(October), 782–785, doi:10.1038/44555.

709 Hasegawa, A., A. Yamamoto, N. Umino, S. Miura, S. Horiuchi, D. Zhao, and H. Sato (2000), Seismic
710 activity and deformation process of the overriding plate in the northeastern Japan subduction
711 zone, *Tectonophysics*, 319(4), 225–239, doi:10.1016/S0040-1951(99)00296-6.

712 Houghton, S. L., G. P. Roberts, I. D. Papanikolaou, and J. M. McArthur (2003), New 234 U- 230 Th
713 coral dates from the western Gulf of Corinth: Implications for extensional tectonics, *Geophys.*
714 *Res. Lett.*, 30(19), 2013, doi:10.1029/2003GL018112.

715 INGV - DISS Working Group (2015), Database of Individual Seismogenic Sources (DISS), Version
716 3.2.0: A compilation of potential sources for earthquakes larger than M 5.5 in Italy and
717 surrounding areas, , doi:10.6092/INGV.IT-DISS3.2.0.

718 Jacques, E., C. Monaco, P. Tapponnier, L. Tortorici, and T. Winter (2001), Faulting and earthquake
719 triggering during the 1783 Calabria seismic sequence, *Geophys. J. Int.*, 147(3), 499–516,
720 doi:10.1046/j.0956-540x.2001.01518.x.

721 Kastens, K. et al. (1988), ODP Leg 107 in the Tyrrhenian Sea: Insights into passive margin and back-

722 arc basin evolution, *Geol. Soc. Am. Bull.*, 100(7), 1140–1156, doi:10.1130/0016-
723 7606(1988)100<1140:OLITTS>2.3.CO;2.

724 King, G. C. P., R. S. Stein, and J. B. Rundle (1988), The Growth of Geological Structures by
725 Repeated Earthquakes 1. Conceptual Framework, *J. Geophys. Res. Solid Earth*, 93(B11),
726 13307–13318, doi:10.1029/JB093iB11p13307.

727 Lucente, F. P., L. Margheriti, C. Piromallo, and G. Barruol (2006), Seismic anisotropy reveals the
728 long route of the slab through the western-central Mediterranean mantle, *Earth Planet. Sci. Lett.*,
729 241(3–4), 517–529, doi:10.1016/j.epsl.2005.10.041.

730 Malinverno, A., and W. B. F. Ryan (1986), Extension in the Tyrrhenian Sea and shortening in the
731 Apennines as result of arc migration driven by sinking of the lithosphere, *Tectonics*, 5(2), 227–
732 245, doi:10.1029/TC005i002p00227.

733 Massonnet, D., and K. L. Feigl (1995), Satellite radar interferometric map of the coseismic
734 deformation field of the M = 6.1 Eureka Valley, California Earthquake of May 17, 1993,
735 *Geophys. Res. Lett.*, 22(12), 1541–1544, doi:10.1029/95GL01088.

736 Massonnet, D., M. Rossi, C. Carmona, F. Adragna, G. Peltzer, K. Feigl, and T. Rabaute (1993), The
737 displacement field of the Landers earthquake mapped by radar interferometry, *Nature*,
738 364(6433), 138–142, doi:10.1038/364138a0.

739 Mastrolembo Ventura, B., E. Serpelloni, A. Argnani, A. Bonforte, R. Bürgmann, M. Anzidei, P.
740 Baldi, and G. Puglisi (2014), Fast geodetic strain-rates in eastern Sicily (southern Italy): New
741 insights into block tectonics and seismic potential in the area of the great 1693 earthquake, *Earth*
742 *Planet. Sci. Lett.*, 404, 77–88, doi:10.1016/j.epsl.2014.07.025.

743 McCloskey, J., S. S. Nalbant, and S. Steacy (2005), Indonesian earthquake: Earthquake risk from co-
744 seismic stress, *Nature*, 434(7031), 291–291, doi:10.1038/434291a.

745 McNeill, L. C., and R. E. L. Collier (2004), Uplift and slip rates of the eastern Eliko fault segment,
746 Gulf of Corinth, Greece, inferred from Holocene and Pleistocene terraces, *J. Geol. Soc. London.*,
747 161(1), 81–92, doi:10.1144/0016-764903-029.

748 Meltzner, A. J., K. Sieh, M. Abrams, D. C. Agnew, K. W. Hudnut, J.-P. Avouac, and D. H.
749 Natawidjaja (2006), Uplift and subsidence associated with the great Aceh-Andaman earthquake

750 of 2004, *J. Geophys. Res. Solid Earth*, 111(B2), n/a-n/a, doi:10.1029/2005JB003891.

751 Michetti, A. M., L. Ferreli, L. Serva, and E. Vittori (1997), Geological evidence for strong historical
752 earthquakes in an “aseismic” region: The Pollino case (Southern Italy), *J. Geodyn.*, 24(1–4), 67–
753 86, doi:10.1016/S0264-3707(97)00018-5.

754 Miyauchi, T., G. Dai Pra, and S. Sylos Labini (1994), Geochronology of Pleistocene marine terraces
755 and regional tectonics in the Tyrrhenian coast of South Calabria, Italy, *Quat.*, 7, 17–34.

756 Monaco, C., and L. Tortorici (2000), Active faulting in the Calabrian arc and eastern Sicily, *J.*
757 *Geodyn.*, 29(3–5), 407–424, doi:10.1016/S0264-3707(99)00052-6.

758 Nalbant, S., J. McCloskey, S. Steacy, M. NicBhloscaidh, and S. Murphy (2013), Interseismic
759 coupling, stress evolution, and earthquake slip on the Sunda megathrust, *Geophys. Res. Lett.*,
760 40(16), 4204–4208, doi:10.1002/grl.50776.

761 Nic Bhloscaidh, M., J. McCloskey, M. Naylor, S. Murphy, and A. Lindsay (2015), Reconstruction of
762 the slip distributions in historical earthquakes on the Sunda megathrust, W. Sumatra, *Geophys. J.*
763 *Int.*, 202(2), 1339–1361, doi:10.1093/gji/ggv195.

764 Nicol, A., and J. Beavan (2003), Shortening of an overriding plate and its implications for slip on a
765 subduction thrust, central Hikurangi Margin, New Zealand, *Tectonics*, 22(6), n/a-n/a,
766 doi:10.1029/2003TC001521.

767 Nigro, F., and A. Sulli (1995), Plio-Pleistocene extensional tectonics in the Western Peloritani area
768 and its offshore (northeastern Sicily), *Tectonophysics*, 252(1–4), 295–305, doi:10.1016/0040-
769 1951(95)00096-8.

770 Nixon, C. W. et al. (2016), Rapid spatiotemporal variations in rift structure during development of the
771 Corinth Rift, central Greece, *Tectonics*, 35(5), 1225–1248, doi:10.1002/2015TC004026.

772 Palano, M., L. Ferranti, C. Monaco, M. Mattia, M. Aloisi, V. Bruno, F. Cannav??, and G. Siligato
773 (2012), GPS velocity and strain fields in Sicily and southern Calabria, Italy: Updated geodetic
774 constraints on tectonic block interaction in the central Mediterranean, *Rend. Online Soc. Geol.*
775 *Ital.*, 21(PART 1), 235–237, doi:10.1029/2012JB009254.

776 Papanikolaou, D., M. Alexandri, and P. Nomikou (2006), Active faulting in the north Aegean basin,
777 in *Special Paper 409: Postcollisional Tectonics and Magmatism in the Mediterranean Region*

778 *and Asia*, pp. 189–209, Geological Society of America.

779 Papanikolaou, I. D., and G. P. Roberts (2007), Geometry, kinematics and deformation rates along the
780 active normal fault system in the southern Apennines: Implications for fault growth, *J. Struct.*
781 *Geol.*, 29(1), 166–188, doi:10.1016/j.jsg.2006.07.009.

782 Papanikolaou, I. D., G. P. Roberts, and A. M. Michetti (2005), Fault scarps and deformation rates in
783 Lazio–Abruzzo, Central Italy: Comparison between geological fault slip-rate and GPS data,
784 *Tectonophysics*, 408(1–4), 147–176, doi:10.1016/j.tecto.2005.05.043.

785 Papanikolaou, I. D., M. Foumelis, I. Parcharidis, E. L. Lekkas, and I. G. Fountoulis (2010),
786 Deformation pattern of the 6 and 7 April 2009, $M_W=6.3$ and $M_W=5.6$ earthquakes in L’Aquila
787 (Central Italy) revealed by ground and space based observations, *Nat. Hazards Earth Syst. Sci.*,
788 10(1), 73–87, doi:10.5194/nhess-10-73-2010.

789 Patacca, E., R. Sartori, and P. Scandone (1990), Tyrrhenian basin and apenninic arcs: kinematic
790 relations since late Tortonian times, *Mem. della Soc. Geol. Ital.*, 45, 425–451.

791 Pepe, F., G. Bertotti, F. Cella, and E. Marsella (2000), Rifted margin formation in the south
792 Tyrrhenian Sea: A high-resolution seismic profile across the north Sicily passive continental
793 margin, *Tectonics*, 19(2), 241–257, doi:10.1029/1999TC900067.

794 Pepe, F., A. Sulli, M. Agate, D. Di Maio, A. Kok, C. Lo Iacono, and R. Catalano (2003), Plio-
795 Pleistocene geological evolution of the northern Sicily continental margin (southern Tyrrhenian
796 Sea): new insights from high-resolution, multi-electrode sparker profiles, *Geo-Marine Lett.*,
797 23(1), 53–63, doi:10.1007/s00367-003-0124-3.

798 Rehault, J.-P., G. Boillot, and A. Mauffret (1984), The Western Mediterranean Basin geological
799 evolution, *Mar. Geol.*, 55(3–4), 447–477, doi:10.1016/0025-3227(84)90081-1.

800 Roberts, G. P., and A. M. Michetti (2004), Spatial and temporal variations in growth rates along
801 active normal fault systems: an example from The Lazio–Abruzzo Apennines, central Italy, *J.*
802 *Struct. Geol.*, 26(2), 339–376, doi:10.1016/S0191-8141(03)00103-2.

803 Roberts, G. P., A. M. Michetti, P. Cowie, N. C. Morewood, and I. Papanikolaou (2002), Fault slip-
804 rate variations during crustal-scale strain localisation, central Italy, *Geophys. Res. Lett.*, 29(8), 9-
805 1-9–4, doi:10.1029/2001GL013529.

806 Roberts, G. P., S. L. Houghton, C. Underwood, I. Papanikolaou, P. A. Cowie, P. van Calsteren, T.
807 Wigley, F. J. Cooper, and J. M. McArthur (2009), Localization of Quaternary slip rates in an
808 active rift in 10 5 years: An example from central Greece constrained by ^{234}U - ^{230}Th coral
809 dates from uplifted paleoshorelines, *J. Geophys. Res.*, *114*(B10), B10406,
810 doi:10.1029/2008JB005818.

811 Roberts, G. P., M. Meschis, S. Houghton, C. Underwood, and R. M. Briant (2013), The implications
812 of revised Quaternary palaeoshoreline chronologies for the rates of active extension and uplift in
813 the upper plate of subduction zones, *Quat. Sci. Rev.*, *78*, 169–187,
814 doi:10.1016/j.quascirev.2013.08.006.

815 Roda-Boluda, D. C., and A. C. Whittaker (2017), Structural and geomorphological constraints on
816 active normal faulting and landscape evolution in Calabria, Italy, *J. Geol. Soc. London.*,
817 jgs2016-097, doi:10.1144/jgs2016-097.

818 Rohling, E. J., G. L. Foster, K. M. Grant, G. Marino, A. P. Roberts, M. E. Tamisiea, and F. Williams
819 (2014), Sea-level and deep-sea-temperature variability over the past 5.3 million years, *Nature*,
820 *508*(7497), 477–482, doi:10.1038/nature13230.

821 Saillard, M., S. R. Hall, L. Audin, D. L. Farber, V. Regard, and G. Hérail (2011), Andean coastal
822 uplift and active tectonics in southern Peru: ^{10}Be surface exposure dating of differentially
823 uplifted marine terrace sequences (San Juan de Marcona, $\sim 15.4^\circ\text{S}$), *Geomorphology*, *128*(3–4),
824 178–190, doi:10.1016/j.geomorph.2011.01.004.

825 Scarfi, L., G. Barberi, C. Musumeci, and D. Patanè (2016a), Seismotectonics of northeastern Sicily
826 and southern Calabria (Italy): New constraints on the tectonic structures featuring in a crucial
827 sector for the central Mediterranean geodynamics, *Tectonics*, *35*(3), 812–832,
828 doi:10.1002/2015TC004022.

829 Scarfi, L., G. Barberi, C. Musumeci, and D. Patanè (2016b), Seismotectonics of northeastern Sicily
830 and southern Calabria (Italy): New constraints on the tectonic structures featuring in a crucial
831 sector for the central Mediterranean geodynamics, *Tectonics*, *35*(3), 812–830,
832 doi:10.1002/2015TC004022.

833 Scicchitano, G., V. Lo Presti, C. R. Spampinato, M. Gasparo Morticelli, F. Antonioli, R. Auriemma,

834 L. Ferranti, and C. Monaco (2011), Millstones as indicators of relative sea-level changes in
835 northern Sicily and southern Calabria coastlines, Italy, *Quat. Int.*, 232(1–2), 92–104,
836 doi:10.1016/j.quaint.2010.08.019.

837 Selvaggi, G., and C. Chiarabba (1995), Seismicity and P-wave velocity image of the Southern
838 Tyrrhenian subduction zone, *Geophys. J. Int.*, 121(3), 818–826, doi:10.1111/j.1365-
839 246X.1995.tb06441.x.

840 Serpelloni, E., M. Anzidei, P. Baldi, G. Casula, and A. Galvani (2005), Crustal velocity and strain-
841 rate fields in Italy and surrounding regions: new results from the analysis of permanent and non-
842 permanent GPS networks, *Geophys. J. Int.*, 161(3), 861–880, doi:10.1111/j.1365-
843 246X.2005.02618.x.

844 Serpelloni, E., G. Vannucci, S. Pondrelli, A. Argnani, G. Casula, M. Anzidei, P. Baldi, and P.
845 Gasperini (2007), Kinematics of the Western Africa-Eurasia plate boundary from focal
846 mechanisms and GPS data, *Geophys. J. Int.*, 169(3), 1180–1200, doi:10.1111/j.1365-
847 246X.2007.03367.x.

848 Serpelloni, E., C. Faccenna, G. Spada, D. Dong, and S. D. P. Williams (2013), Vertical GPS ground
849 motion rates in the Euro-Mediterranean region: New evidence of velocity gradients at different
850 spatial scales along the Nubia-Eurasia plate boundary, *J. Geophys. Res. Solid Earth*, 118(11),
851 6003–6024, doi:10.1002/2013JB010102.

852 Siddall, M., E. J. Rohling, A. Almogi-Labin, C. Hemleben, D. Meischner, I. Schmelzer, and D. A.
853 Smeed (2003), Sea-level fluctuations during the last glacial cycle, *Nature*, 423(6942), 853–858,
854 doi:10.1038/nature01690.

855 Spampinato, C. R., G. Scicchitano, L. Ferranti, and C. Monaco (2012), Raised Holocene paleo-
856 shorelines along the Capo Schisò coast, Taormina: New evidence of recent co-seismic
857 deformation in northeastern Sicily (Italy), *J. Geodyn.*, 55, 18–31, doi:10.1016/j.jog.2011.11.007.

858 Stewart, I. S., A. Cundy, S. Kershaw, and C. Firth (1997), Holocene coastal uplift in the taormina
859 area, northeastern sicily: Implications for the southern prolongation of the calabrian seismogenic
860 belt, *J. Geodyn.*, 24(1–4), 37–50, doi:10.1016/S0264-3707(97)00012-4.

861 Stucchi, M. et al. (2013), The SHARE European Earthquake Catalogue (SHEEC) 1000–1899, *J.*

862 *Seismol.*, 17(2), 523–544, doi:10.1007/s10950-012-9335-2.

863 Sulli, A., V. Lo Presti, M. Gasparo Morticelli, and F. Antonioli (2013), Vertical movements in NE
864 Sicily and its offshore: Outcome of tectonic uplift during the last 125 ky, *Quat. Int.*, 288, 168–
865 182, doi:10.1016/j.quaint.2012.01.021.

866 Tarquini, S., I. Isola, M. Favalli, F. Mazzarini, M. Bisson, M. T. Pareschi, and E. Boschi (2007),
867 TINITALY/01: A new Triangular Irregular Network of Italy, *Ann. Geophys.*, 50(3), 407–425.

868 Tarquini, S., S. Vinci, M. Favalli, F. Doumaz, A. Fornaciai, and L. Nannipieri (2012), Release of a
869 10-m-resolution DEM for the Italian territory: Comparison with global-coverage DEMs and
870 anaglyph-mode exploration via the web, *Comput. Geosci.*, 38(1), 168–170,
871 doi:10.1016/j.cageo.2011.04.018.

872 Tortorici, G., M. Bianca, G. De Guidi, C. Monaco, and L. Tortorici (2003), Fault activity and marine
873 terracing in the Capo Vaticano area (southern Calabria) during the Middle-Late Quaternary,
874 *Quat. Int.*, 101–102(1), 269–278, doi:10.1016/S1040-6182(02)00107-6.

875 Tortorici, L., C. Monaco, C. Tansi, and O. Cocina (1995), Recent and active tectonics in the Calabrian
876 arc (Southern Italy), *Tectonophysics*, 243(1–2), 37–55, doi:10.1016/0040-1951(94)00190-K.

877 Trincardi, F., and N. Zitellini (1987), The rifting of the Tyrrhenian Basin, *Geo-Marine Lett.*, 7(1), 1–
878 6, doi:10.1007/BF02310459.

879 Vacchi, M., A. Rovere, N. Zouros, S. Desruelles, V. Caron, and M. Firpo (2012), Spatial distribution
880 of sea-level markers on Lesvos Island (NE Aegean Sea): Evidence of differential relative sea-
881 level changes and the neotectonic implications, *Geomorphology*, 159–160, 50–62,
882 doi:10.1016/j.geomorph.2012.03.004.

883 Valensise, G., and D. Pantosti (1992), A 125 Kyr-long geological record of seismic source
884 repeatability: the Messina Straits (southern Italy) and the 1908 earthquake ($M_s 7/2$), *Terra*
885 *Nov.*, 4(4), 472–483, doi:10.1111/j.1365-3121.1992.tb00583.x.

886 Walters, R. J., J. R. Elliott, N. D’Agostino, P. C. England, I. Hunstad, J. A. Jackson, B. Parsons, R. J.
887 Phillips, and G. Roberts (2009), The 2009 L’Aquila earthquake (central Italy): A source
888 mechanism and implications for seismic hazard, *Geophys. Res. Lett.*, 36(17), L17312,
889 doi:10.1029/2009GL039337.

890 Ward, S. N. (1998), On the consistency of earthquake moment release and space geodetic strain rates:
891 Europe, *Geophys. J. Int.*, *135*, 1011–1018, doi:10.1046/j.1365-246X.1998.00658.x.

892 Wells, D. L., and K. J. Coppersmith (1994), New empirical relationships among magnitude, rupture
893 length, rupture width, rupture area, and surface displacement, *Bull. Seismol. Soc. Am.*, *84*(4),
894 974–1002.

895 Westaway, R. (1993), Quaternary uplift of southern Italy, *J. Geophys. Res.*, *98*(B12), 741–772,
896 doi:10.1029/93JB01566.

897 Wortel, M. J., and W. Spakman (2000), Subduction and slab detachment in the Mediterranean-
898 Carpathian region., *Science*, *290*(5498), 1910–1917, doi:10.1126/science.290.5498.1910.

899 Yeats, R. (2012), *Active Faults of the World*, Cambridge University Press, Cambridge.

900 Yeats, R. S., and C. S. Prentice (1996), Introduction to Special Section: Paleoseismology, *J. Geophys.*
901 *Res. Solid Earth*, *101*(B3), 5847–5853, doi:10.1029/95JB03134.

902

903 **Table 1**

Reference	Dating Method	Dated sample description	Profile number	Reported Age (ky)	Assigned Highstand (ka)	Palaeo-shoreline Elevation (m a.s.l)
Scicchitano et al., 2011 and Sulli et al., 2013	U/Th dating	<i>“A shell of Spondylus sp collected within thick marine deposit constituted by coarse polygenic conglomerates, micro-conglomerates and crossed lamination sands.”</i>	6	100 - 125	125	53
Giunta et al., 2012	OSL dating	<i>“Yellow shore sands from unconsolidated marine sands.”</i>	10	118 ± 7	125	61
Giunta et al., 2012	OSL dating	<i>“Sandy levels from unconsolidated marine sands.”</i>	14/15	283 ± 22	285	208

904 **Table 1** – Previous dating of palaeoshorelines lying within the investigated area by Scicchitano et al.

905 [2011], Giunta et al. [2012] and Sulli et al. [2013]. Note that different dating methods have confirmed

906 the age (125 ky) of a prominent marine terrace along the strike of fault and over its tip. Details about
 907 their location are shown in Figure 2a and b.

908

909 **Table 2**

Palaeoshoreline (Profile number)	DEMs Elevations (m)	Expected Elevations (m)	Field Elevations (m)	Giunta's Elevations (m)	Our proposed Age (kyrs)	Age proposed by Giunta et al., 2012 (kyrs)	UTM Coordinate
3 (1)	57	59	-	57	125	125	33 S 0475871 4219672
7 (1)	99	99	-	99	240	200	33 S 0476308 4219436
3 (2)	57	59	-	57	125	125	33 S 0474722 4217578
7 (2)	98	98	-	98	240	200	33 S 0475083 4217269
3 (3)	54	54	-	54	125	125	33 S 0474353 4217219
7 (3)	87	89	-	87	240	200	33 S 0474511 4216876
3 (4)	49	50	-	49	125	125	33 S 0473994 4216902
7 (4)	80	79	-	-	240	-	33 S 0474049 4216761
10 (4)	124	124	-	124	340	200	33 S 0474265 4216425
3 (5)	51	51	50	51	125	125	33 S 0473639 4216783
7 (5)	81	84	85	-	240	-	33 S 0473912 4216612
9 (5)	98	93	-	98	310	200	33 S 0473868 4216424
10 (5)	125	131	120	-	340	-	33 S 0473996 4216277
3 (6)	53	53	50	53	125	125	33 S 0472871 4216042
7 (6)	83	86	85	-	240	-	33 S 0473005 4215984
9 (6)	100	96	110	100	310	200	33 S 0473260 4215861
3 (7)	54	51	-	54	125	125	33 S 0472915 4215755
10 (7)	129	131	-	129	340	200	33 S 0473105 4215415

3 (8)	56	56	-	56	125	125	33 S 0472539 4215404
7 (8)	96	93	-	96	240	200	33 S 0472701 4215060
3 (9)	55	54	54	55	125	125	33 S 0471586 4215093
7 (9)	88	89	75	88	240	200	33 S 0471462 4214794
9 (9)	102	99	100	-	310	-	33 S 0471767 4214611
3 (10)	61	63	-	61	125	125	33 S 0470269 4213855
7 (10)	105	105	115	105	240	200	33 S 0470442 4213664
9 (10)	123	121	-	-	310	-	33 S 0470528 4213527
10 (10)	152	161	145	-	340	-	33 S 0470823 4213768
1 (11)	26	21	-	-	76	-	33 S 0469214 4213892
2 (11)	50	42	-	50	100	76	33 S 0469289 4213580
3 (11)	87	89	-	87	125	125	33 S 0469370 4213279
5 (11)	125	129	-	125	200	200	33 S 0469435 4213057
7 (11)	150	156	-	-	240	-	33 S 0469528 4212622
9 (11)	190	186	-	-	310	-	33 S 0469673 4212322
10 (11)	230	233	-	-	340	-	33 S 0469861 4212020
11 (11)	274	270	-	-	410?	-	33 S 0470076 4211665
1 (12)	25	28	-	25	76	76 (?)	33 S 0468440 4213543
2 (12)	50	51	-	50	100	76 (?)	33 S 0468458 4213177
3 (12)	100	100	-	100	125	125	33 S 0468478 4212907
6 (12)	143	147	-	-	200	-	33 S 0468480 4212536
7 (12)	180	177	-	180	240	200	33 S 0468453 4212205
10 (12)	264	263	-	264	340	340	33 S 0468424 4211752
2 (13)	52	57	-	52	100	76	33 S 0467832 4213228

3 (13)	105	108	-	105	125	125	33 S 0467886 4212584
6 (13)	149	159	-	140 (?)	200	200 (?)	33 S 0467996 4212239
7 (13)	200	192	-	-	240	-	33 S 0468052 4211966
9 (13)	228	232	-	-	310	-	33 S 0468046 4211866
10 (13)	291	284	278	300	340	340	33 S 0467955 4211523
1 (14)	27	33	-	40	76	76 (?)	33 S 0467030 4213264
2 (14)	64	57	-	64	100	76 (?)	33 S 0467078 4212875
3 (14)	109	108	-	109	125	125	33 S 0467227 4212394
6 (14)	155	159	-	146 (?)	200	200 (?)	33 S 0467206 4212147
7 (14)	187	192	-	-	240	-	33 S 0467153 4211987
8 (14)	208	204	-	208	285	285	33 S 0467140 4211866
10 (14)	288	284	-	288	340	340	33 S 0467020 4211313
1 (15)	40	38	-	40	76	76 (?)	33 S 0466553 4213014
2 (15)	61	64	-	61	100	76 (?)	33 S 0466577 4212733
3 (15)	112	116	-	112	125	125	33 S 0466629 4212216
5 (15)	174	173	-	174	200	200	33 S 0466644 4211888
8 (15)	225	224	-	225	285	285	33 S 0466664 4211696
9 (15)	253	254	-	253	310	340	33 S 0466677 4211574

910 **Table 2** - We show all mapped inner edges from DEM and fieldwork with age assigned via
911 synchronous correlation. This table also shows different ages sequentially-assigned by *Giunta et al.*
912 [2012] leading them to derive fluctuating uplift rate values through time. Note that we were unable to
913 check all locations of inner edges mapped through DEM analysis in the field because the investigated
914 area is thickly-vegetated and densely-populated with private properties.

915

916 **Table 3**

Age (ka)	Elevation of highstands (mm)
0	0
30	-80000
50	-60000
76	-30000
100	-25000
125	5000
175	-30000
200	-5000
217	-30000
240	-5000
285	-30000
310	-22000
340	5000
410	-5000

917 **Table 3** - Values of sea-level highstands derived from *Siddall et al.* [2003] used to calculate predicted
918 palaeoshoreline elevations given a value for uplift rate.

919

920 **Figure captions**

921 **Figure 1.** Location map showing the tectonic setting of Calabria and NE Sicily. Pink dots represent
922 locations for historical earthquakes with the associated earthquake magnitude from *Guidoboni et al.*
923 [2007]. Yellow dots show Holocene uplift rate values by *Antonioli et al.*, [2006, 2009]. White-
924 coloured dashed square shows the investigated area. Reported active normal faults are from *Michetti*
925 *et al.*, [1997], *Monaco and Tortorici*, [2000], *Bianca et al.* [2011], *Giunta et al.* [2012] and *Roberts et*
926 *al.*, [2013]: MrF: Maratea Fault, PoF: Pollino Fault, CrF: Crati Fault, RoF: Rossano Fault VF: Vibo
927 Fault, TrF: Tropea Fault, CoF: Coccorino Fault, MF: Mileto Fault, SeF: Serre Fault, CF: Cittanova
928 Fault, SeF: Sant'Eufemia Fault, ScF: Scilla Fault, AF: Armo Fault, RCF: Reggio Calabria Fault, TF:
929 Taormina Fault, AcF: Acireale Fault, CDOF: Capo D'Orlando Fault, SBT: Sicilian Basal Thrust. Note
930 that the CDF (Capo D'Orlando Fault) has not been reported within DISS as shown in inset b. In inset
931 c amended tomographic cross-section from the Gulf of Lion to the Calabrian Arc by [*Lucente et al.*,
932 2006] is shown. Section trace A-B shows the Ionian slab beneath the Calabrian Arc characterized by
933 intermediate and deep earthquakes (white dots).

934

935 **Figure 2.** Location maps for palaeoshorelines within the hangingwall of the Capo d'Orlando active
936 normal fault. A 10-m resolution DEMs with the associated coloured Slope to highlight breaking-

937 slopes is used as base-map. In (a) is shown amended map from *Giunta et al.* [2012] showing the
938 investigated area from Capo d'Orlando town to Santa Agata di Militello town. Location and ages of
939 marine terraces from *Giunta et al.* [2012] are shown as well as locations of U/Th dating and OSL
940 dating by *Scicchitano et al.* [2011] and *Giunta et al.* [2012]. In (b) inner edges of marine terraces with
941 our reviewed ages (see numbered dots and the associated age within Legends panel), the “tip zone”
942 area marked in the SW with red-coloured dashed line and 15-topographic profile locations are shown
943 from this study.

944

945 **Figure 3.** View of interpreted marine terraces in the field (shaded polygons) within the Profile 8 with
946 the associated inner edge elevations and the synchronously-assigned ages. The synchronous
947 correlation approach allowed us to reassign the age of 240 ky to the palaeoshoreline at 96 m
948 previously [*Giunta et al.*, 2012] sequentially-assigned to the 200 ka sea-level highstand.

949

950 **Figure 4.** Field evidence, lying along Profile 6, of inner edge showing upper palaeoshoreface
951 depositional environment. The picture shows a marine abrasion platform made of Mesozoic limestone
952 unconformably overlain by marine conglomeratic deposits already well-described by *Scicchitano et*
953 *al.* [2011] and *Giunta et al.* [2012]. In places lithophagid borings into Mesozoic limestone and
954 scattered evidence of beach cobbles have been mapped close this area, suggesting the presence of the
955 125ka-dated palaeoshoreline. This inner edge could have not been mapped in the DEMs due to the
956 resolution.

957

958 **Figure 5.** Example of a modelled topographic profile (profile 8 herein) showing a synchronously-
959 modelled sequence of marine terraces on the hangingwall of the Capo D'Orlando Fault by iterating
960 uplift rates values to find the best match between mapped palaeoshorelines (using GIS analysis and/or
961 fieldwork) and the predicted sea-level highstands (coloured lines). RMS deviation vs Uplift rates
962 (mm/yr) is shown, suggesting that our preferred uplift rate is very robust. Note that our “best fit” is
963 based on the fact that the iteration of uplift rate values is driven by a dated horizon/palaeoshoreline

964 (125 ka). RMS deviation calculations for each topographic profile are shown in the Supplementary
965 material.

966

967 **Figure 6.** Topographic profiles derived by using 10-m high-resolution Digital Elevation Models
968 [Tarquini *et al.*, 2007, 2012] showing modelled and mapped palaeoshoreline elevations. The coloured
969 lines represent the sea-level highstands (or predicted palaeoshoreline elevations) calculated by
970 iterating uplift rate values to find the best match with the mapped (numbered arrows)
971 palaeoshorelines. More detailed profiles locations on Figure 2b. Inner edge elevations with refined
972 ages are also shown in Table 2

973

974 **Figure 7.** In (a) the graph is showing the relationship between field-based and DEM-based inner edge
975 elevations. The R^2 value > 0.99 confirms a very robust relationship suggesting that elevations
976 measured elsewhere in the DEM are likely to be accurate. In (b) the graph is showing linear
977 regression analysis between our measured and predicted elevations. The predicted elevations,
978 representing the synchronously-calculated sea-level highstand elevations, have been derived by
979 defining a constant uplift rate through time, and iterating this value to find the best match to the
980 measured and mapped palaeoshorelines.

981

982 **Figure 8.** Diagrams showing evidence of Quaternary Capo D'Orlando Fault activity. In (a) uplift rates
983 is spatially varying along strike the Capo D'Orlando Fault. In (b) palaeoshoreline elevations are
984 changing along the strike of the Capo D'Orlando Fault. Solid lines represent our mapped and
985 measured palaeoshoreline elevations mapped by using DEMs and checked in the field; closely-dashed
986 coloured lines represent modelled iteratively-calculated sea-level highstand elevations (or the
987 expected elevations) mostly matching with the solid lines. Uplift/Subsidence ratio (U:S) value of 1/3.5
988 has been applied to the oldest (340 ka) palaeoshoreline mapped within the hangingwall to estimate the
989 expected elevation on the footwall and derive long-term fault slip-rate. A black dashed arrowed line
990 shows the displacement between terraces mapped in the hangingwall and footwall cut-offs. In (c) the
991 faulting activity of Capo D'Orlando Fault over the Late Quaternary has tilted the investigated marine

992 terraces; in fact, older and higher palaeoshorelines show higher tilt angle values because they have
993 been experiencing a longer history of faulting activity.

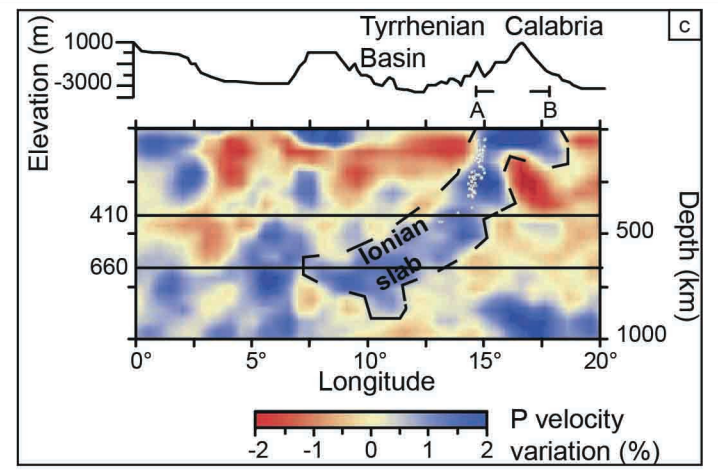
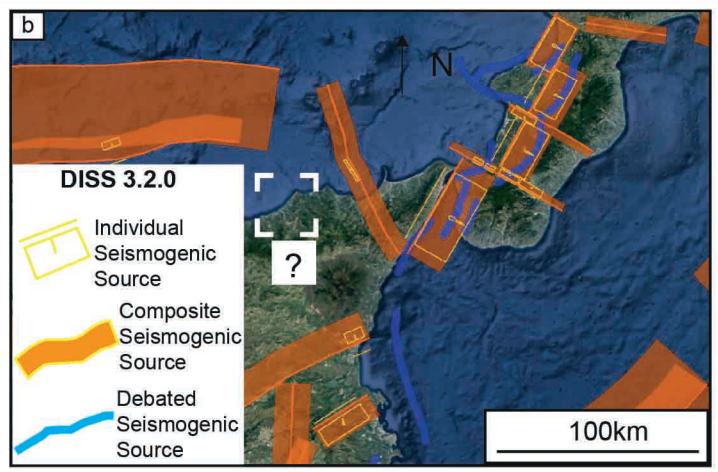
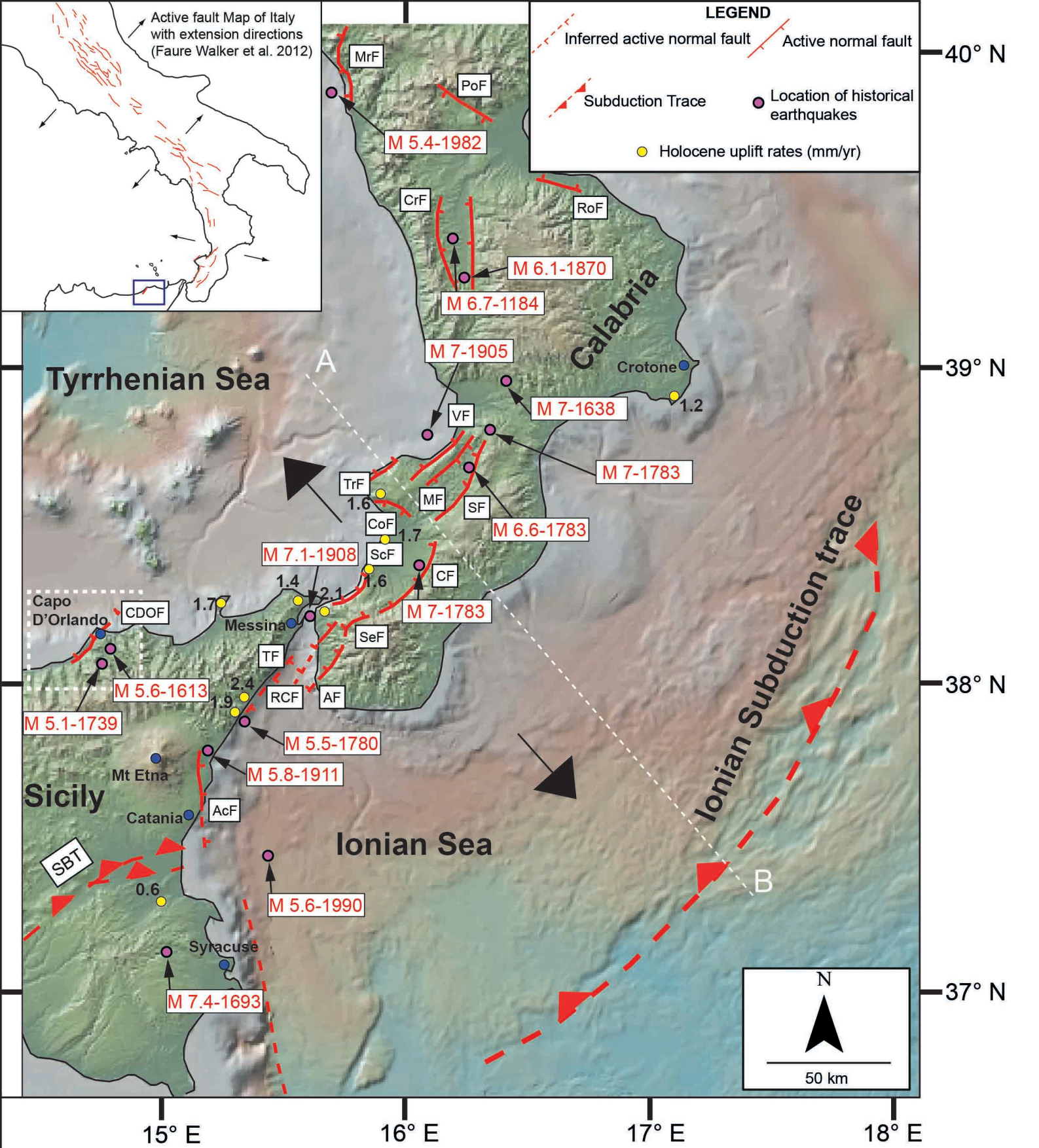
994

995 **Figure 9.** In (a) uplift gradients are shown derived from [Giunta *et al.*, 2012] (orange-coloured
996 dashline) and this study (blue line). The orange-coloured dash line shows an exponential growth of
997 the uplift gradient through time driven by an absolutely-dated palaeoshoreline (125 ka). Instead, the
998 blue-coloured line shows a constant growth of the uplift gradient through time also driven by an
999 absolutely-dated palaeoshoreline (125 ka). Note that changing uplift rates through time is also shown in
1000 Figure 7 (section 2) in Giunta *et al.*, [2012].

1001

1002 **Figure 10.** Regional extension accommodated by normal faults within the upper plate of the Ionian
1003 Subduction Zone, along the geological domain of Calabrian Arc, is shown. In (a) prominent changing
1004 uplift rates from GPS analysis (light blue values) [Serpelloni *et al.*, 2013] are shown along the
1005 Calabrian Arc. Similarly, in (b) Late Quaternary uplift rates change by up to a factor of 4 across the
1006 Calabrian Arc, with large variations between the footwalls and hangingwall of faults, and along the
1007 strike of faults towards fault tips, suggesting prominent heterogeneity for slip on subduction interface
1008 through time.

1009 Light blue values in b are reported by Catalano and De Guidi, [2003] and Ferranti *et al.* [2006], and
1010 black values are reported from this study (black square) and Roberts *et al.* [2013].



Dataset from *Giunta et al. [2012]*

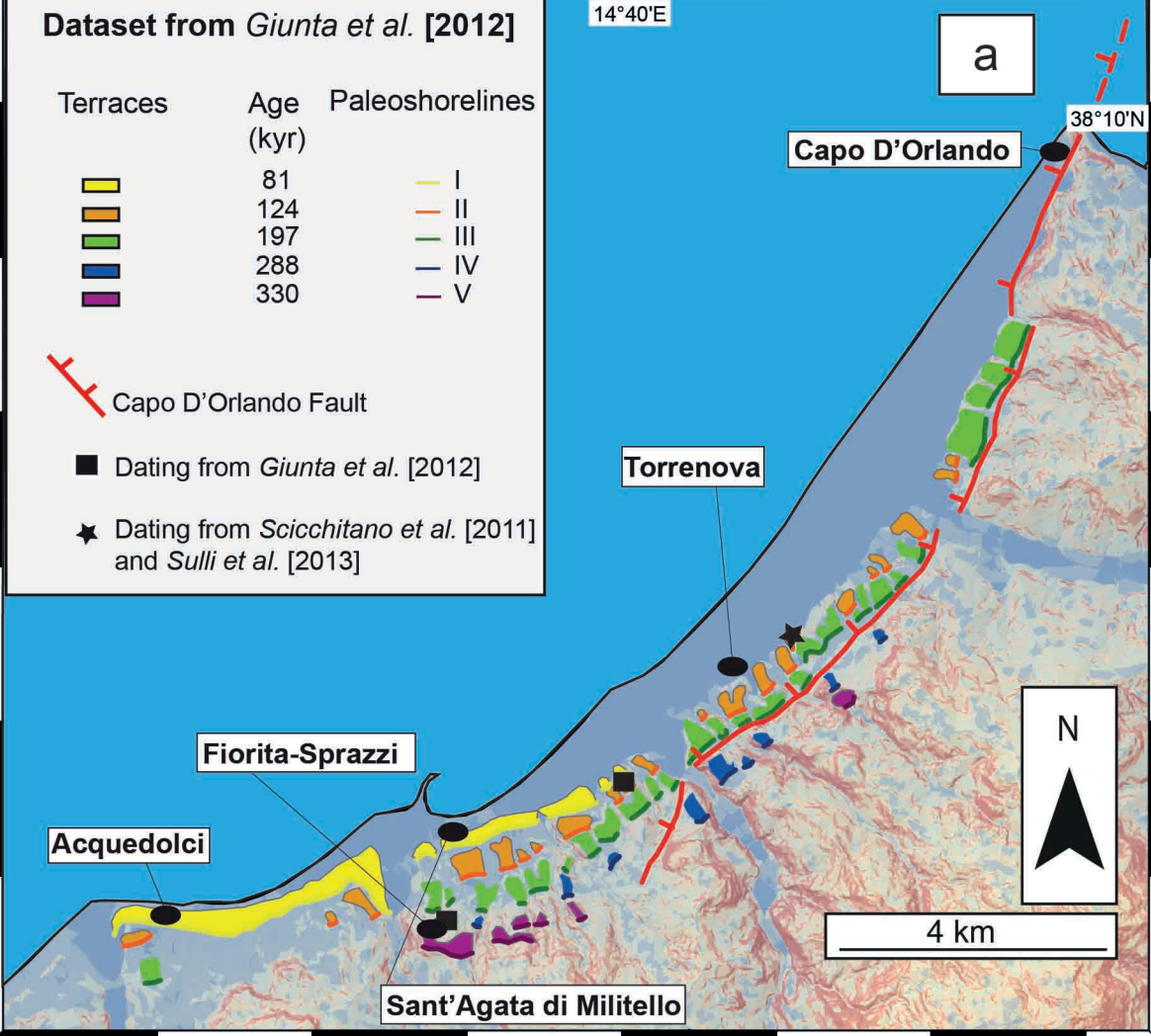
14°40'E

Terraces	Age (kyr)	Paleoshorelines
	81	I
	124	II
	197	III
	288	IV
	330	V

Capo D'Orlando Fault

Dating from *Giunta et al. [2012]*

Dating from *Scicchitano et al. [2011]* and *Sulli et al. [2013]*



LEGENDS

Inner edges and Age (kyr)

- 1 • 76.5
- 2 • 100
- 3 • 125
- 4 • 178
- 5 • 200
- 6 • 217
- 7 • 240
- 8 • 285
- 9 • 310
- 10 • 340

Capo D'Orlando Fault

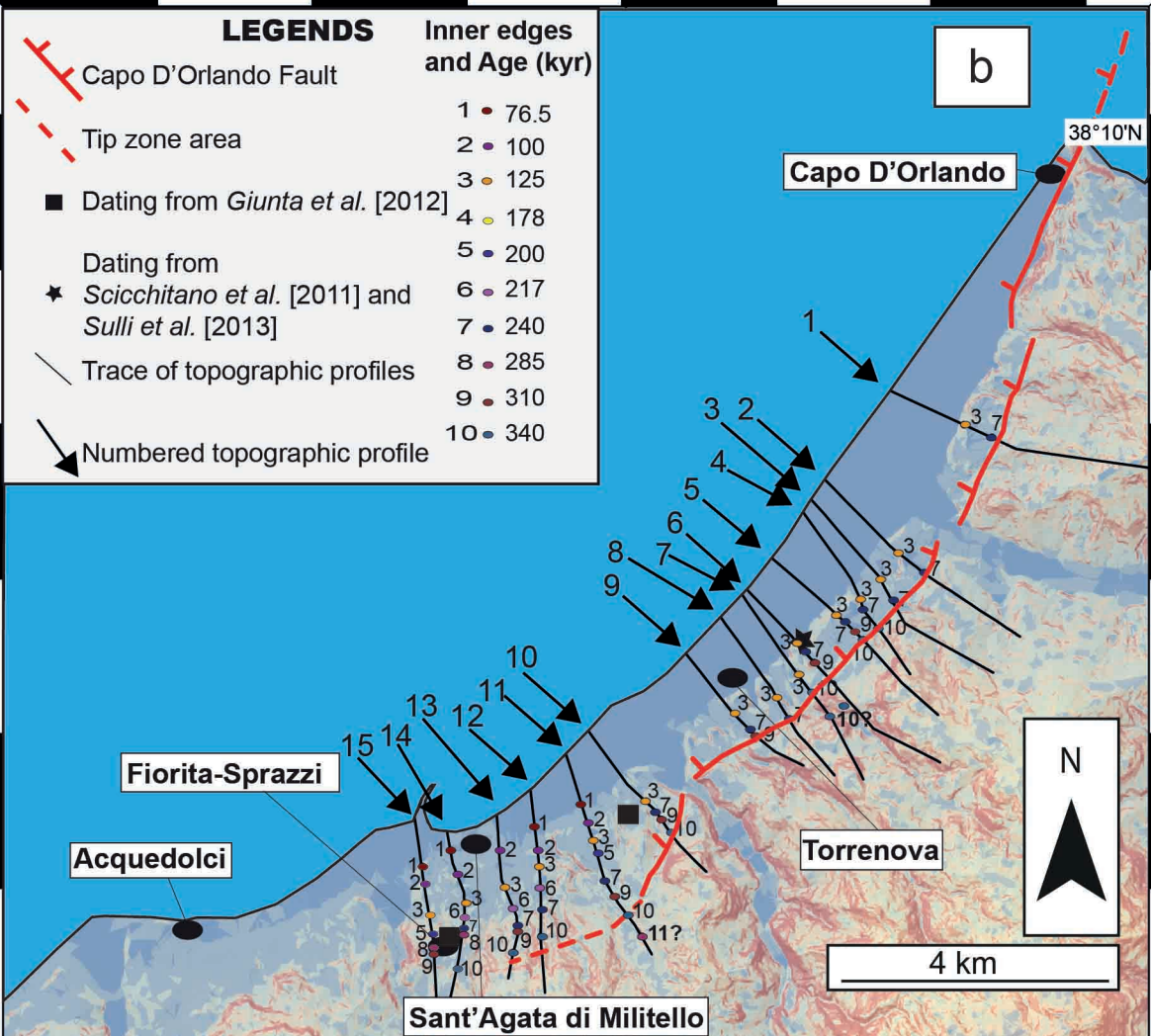
Tip zone area

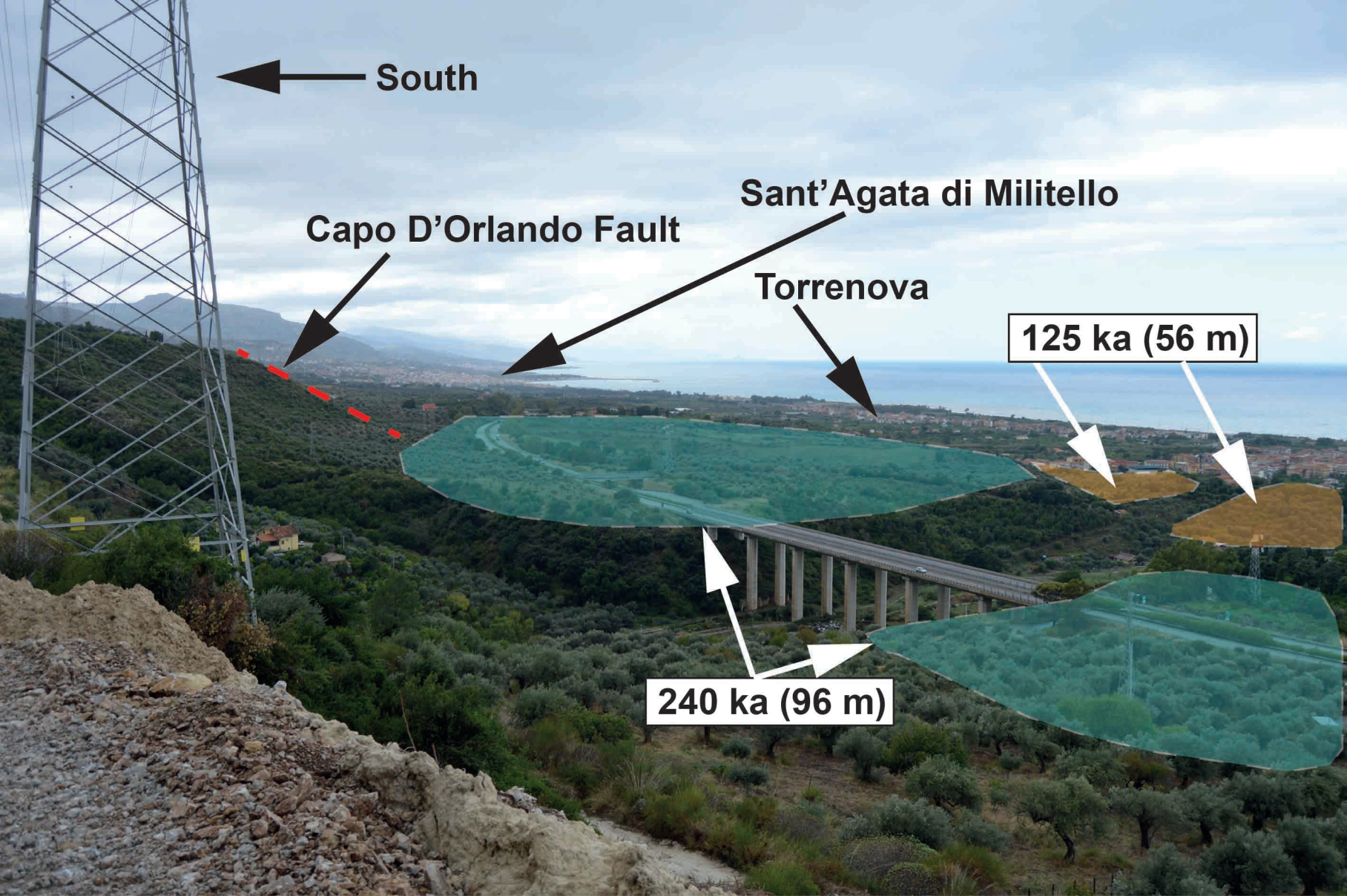
Dating from *Giunta et al. [2012]*

Dating from
Scicchitano et al. [2011] and
Sulli et al. [2013]

Trace of topographic profiles

Numbered topographic profile





← South

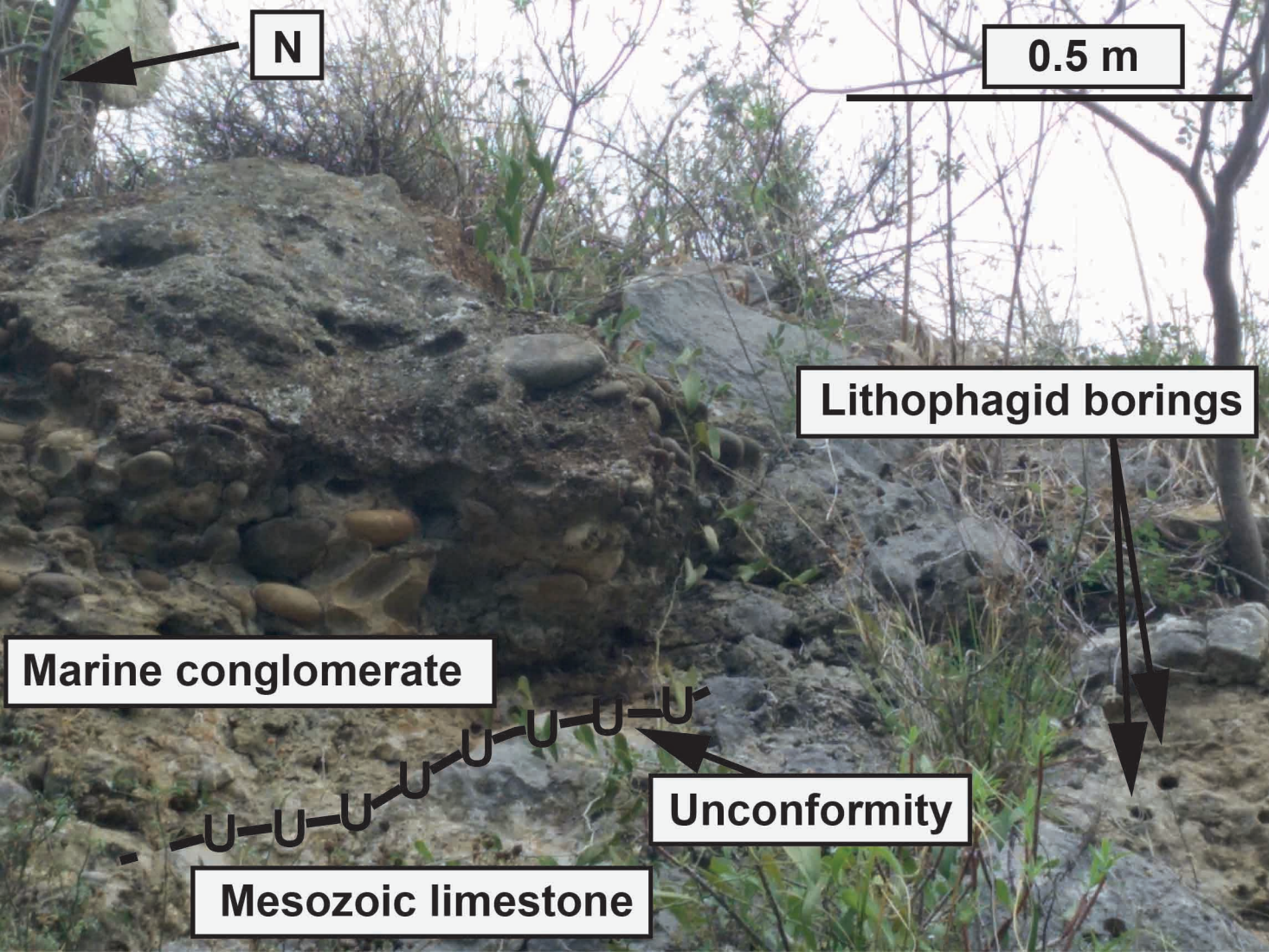
Capo D'Orlando Fault

Sant'Agata di Militello

Torrenova

125 ka (56 m)

240 ka (96 m)



N

0.5 m

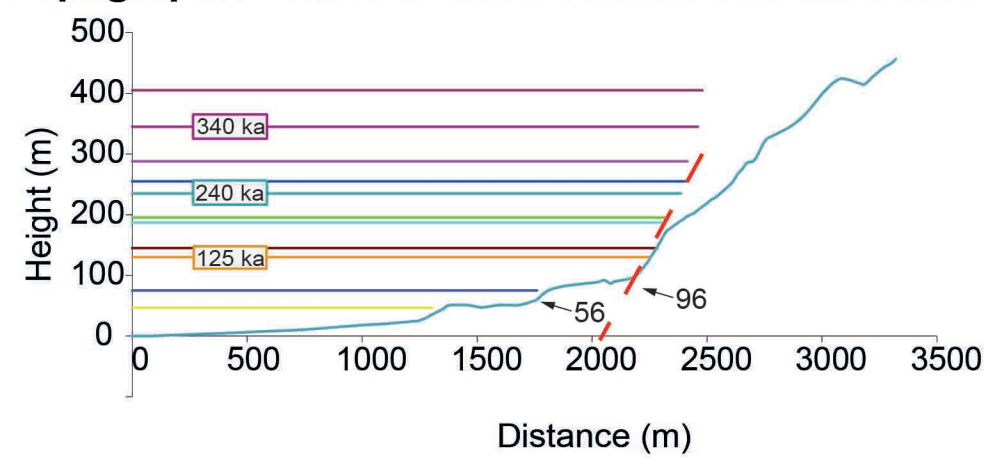
Lithophagid borings

Marine conglomerate

Mesozoic limestone

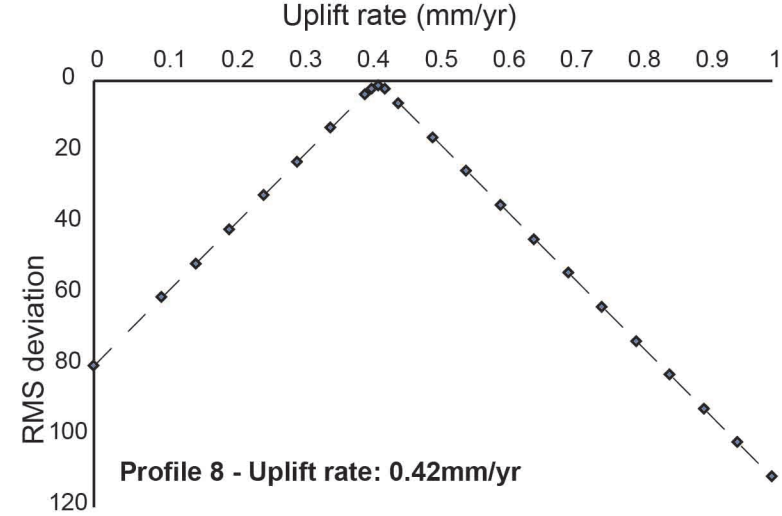
Unconformity

Topographic Profile 8 with modelled shoreline elevations



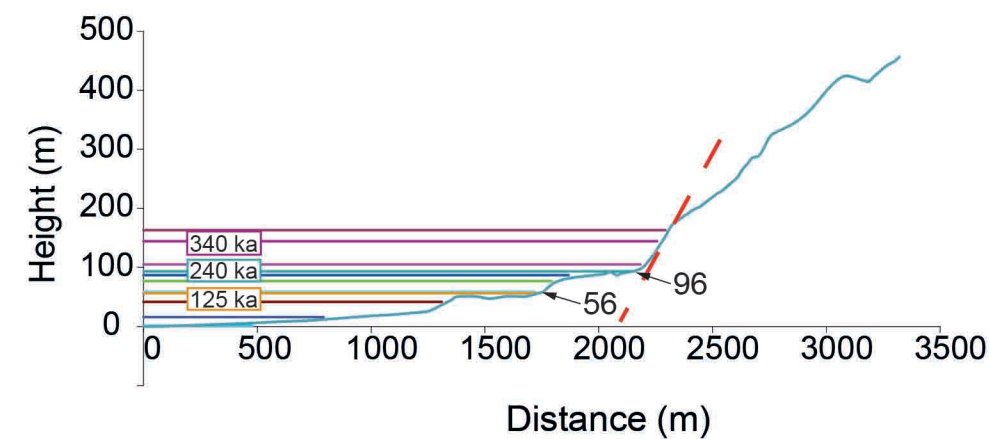
Poor Fit

Uplift rate: 1.0 mm/yr



Profile 8 - Uplift rate: 0.42mm/yr

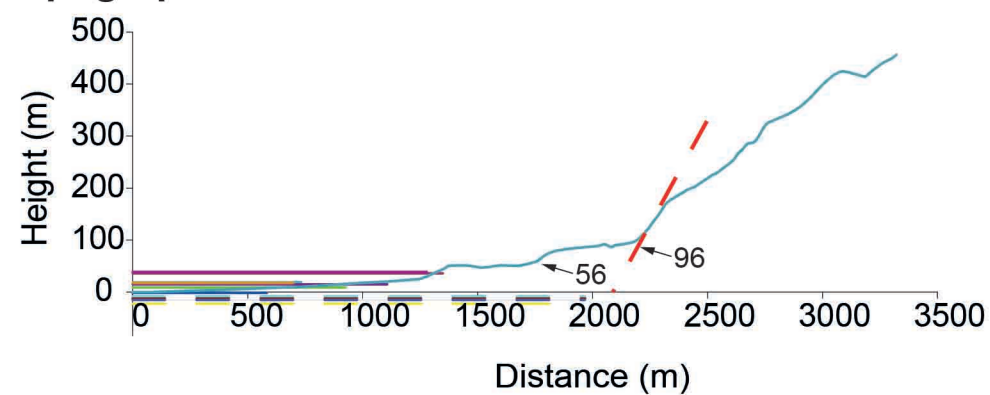
Topographic Profile 8 with modelled shoreline elevations



Best Fit

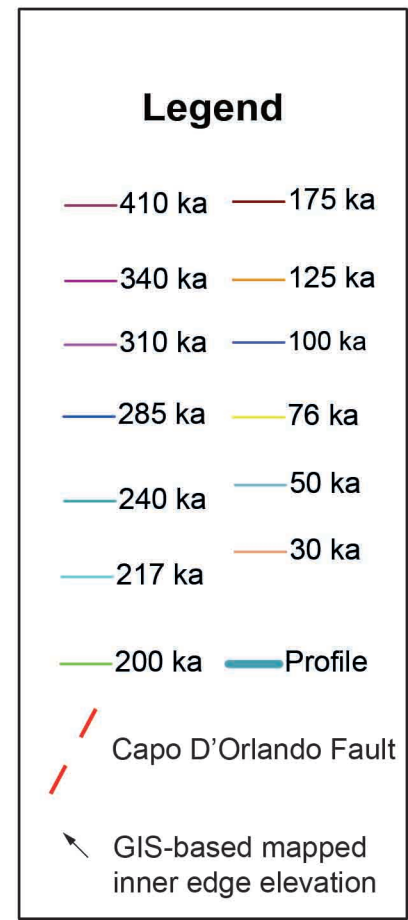
Uplift rate: 0.42 mm/yr

Topographic Profile 8 with modelled shoreline elevations

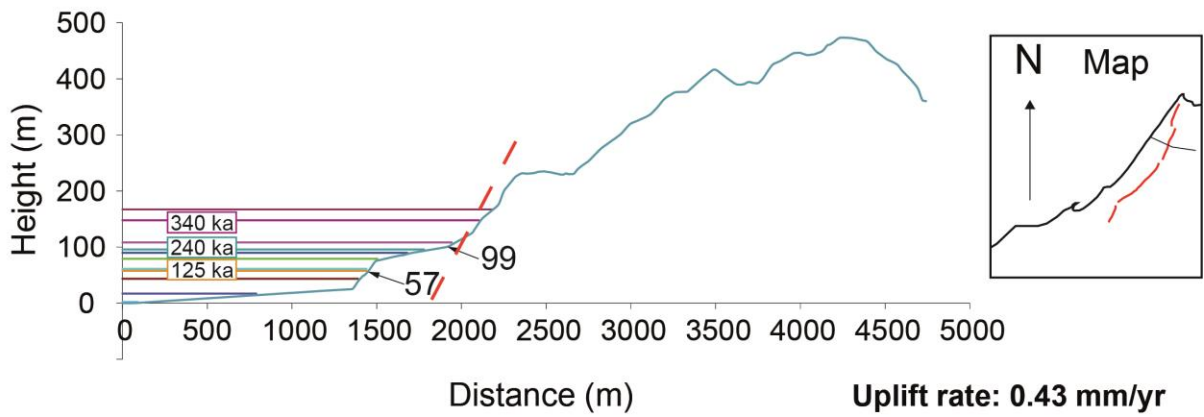


Poor Fit

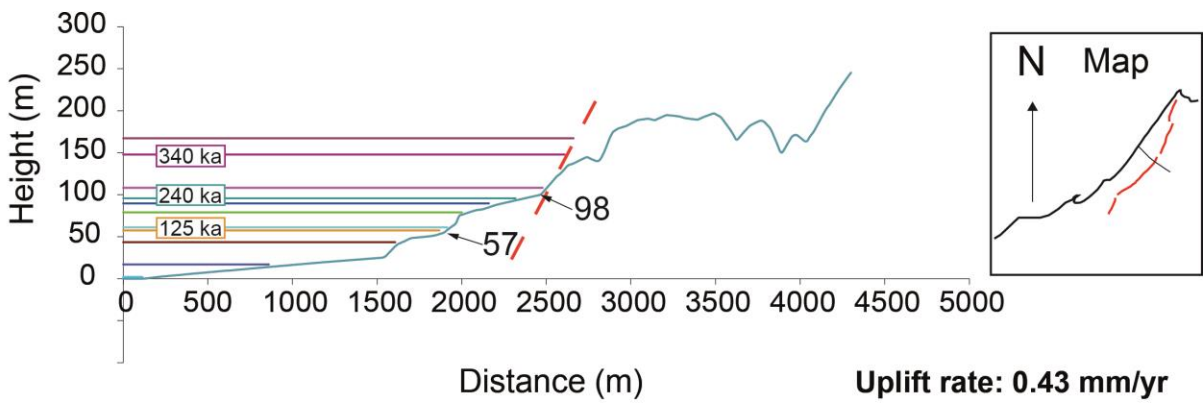
Uplift rate: 0.1 mm/yr



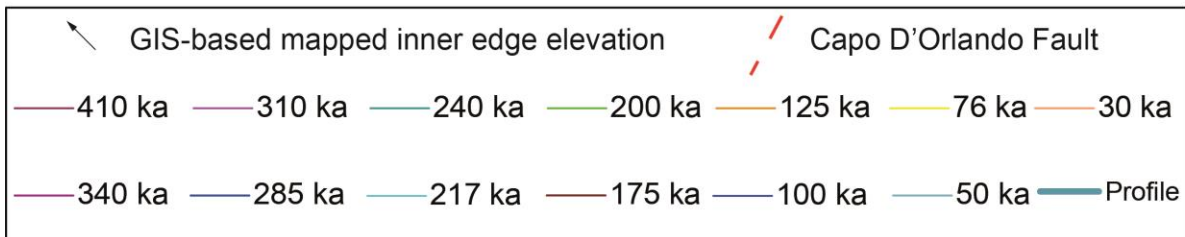
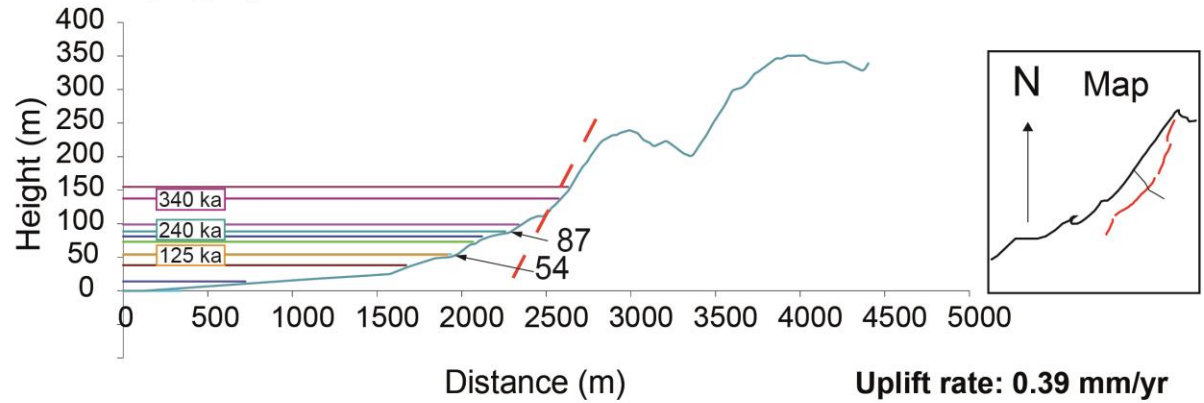
Topographic Profile 1 with modelled shoreline elevations



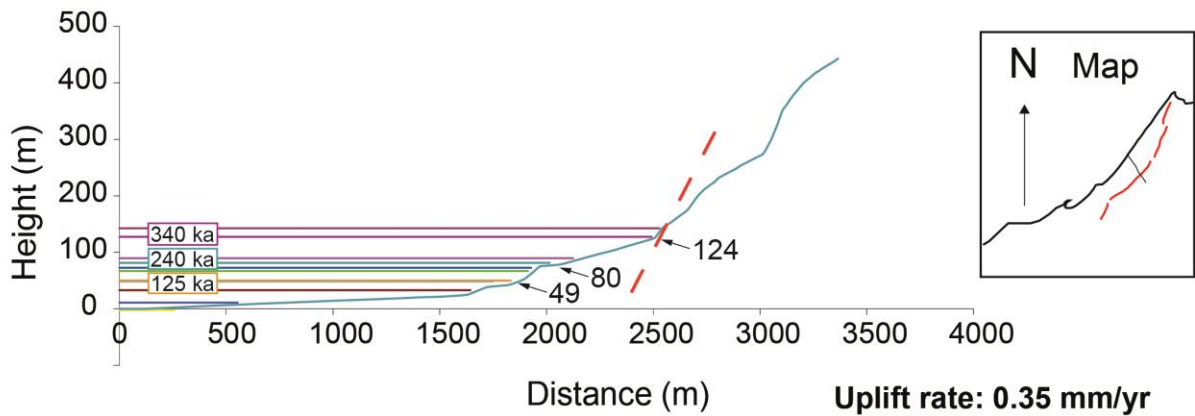
Topographic Profile 2 with modelled shoreline elevations



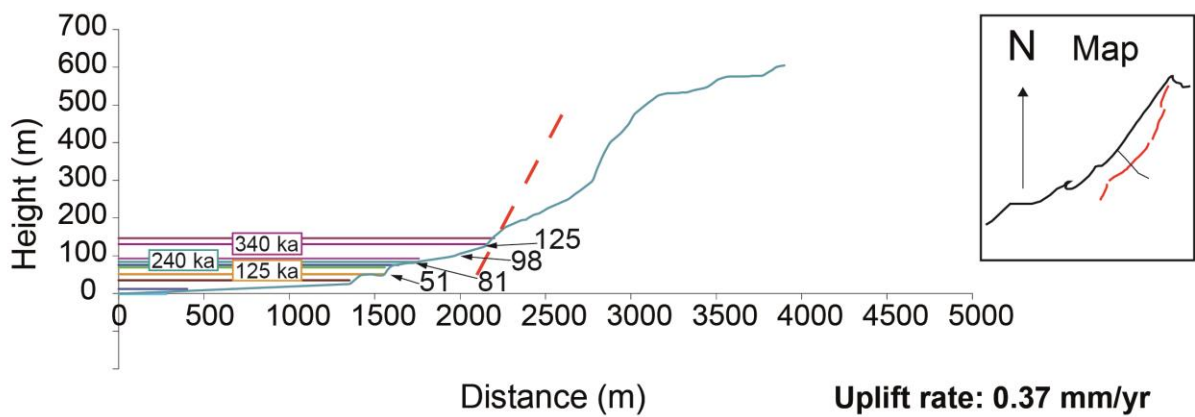
Topographic Profile 3 with modelled shoreline elevations



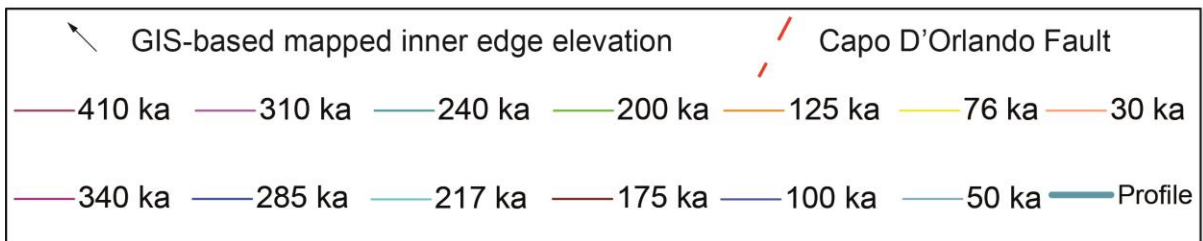
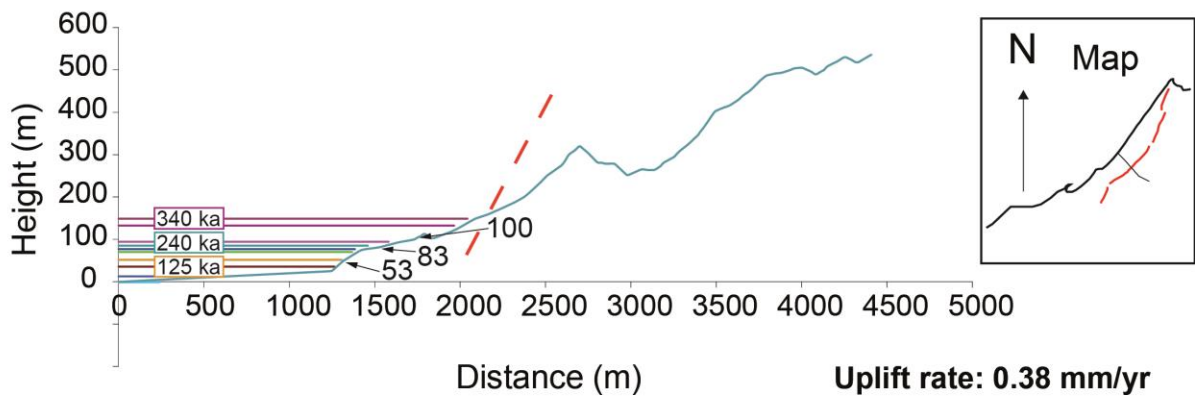
Topographic Profile 4 with modelled shoreline elevations



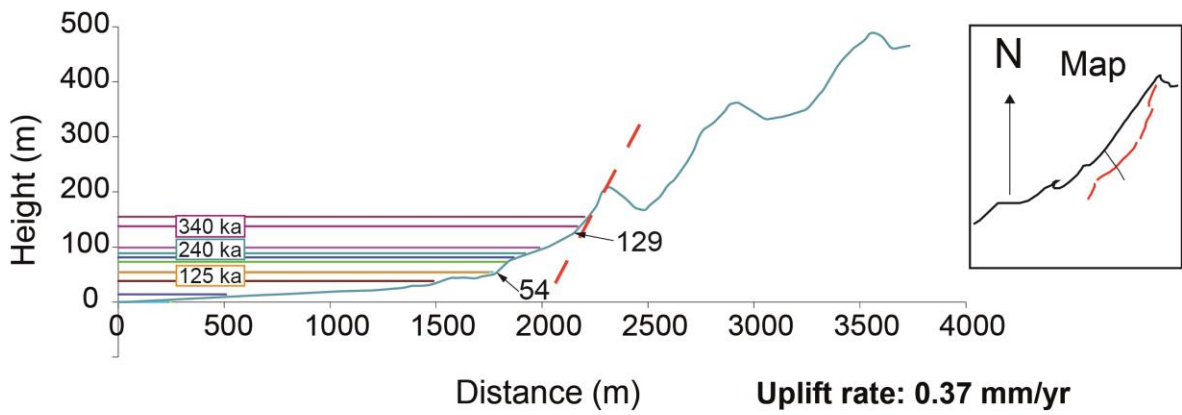
Topographic Profile 5 with modelled shoreline elevations



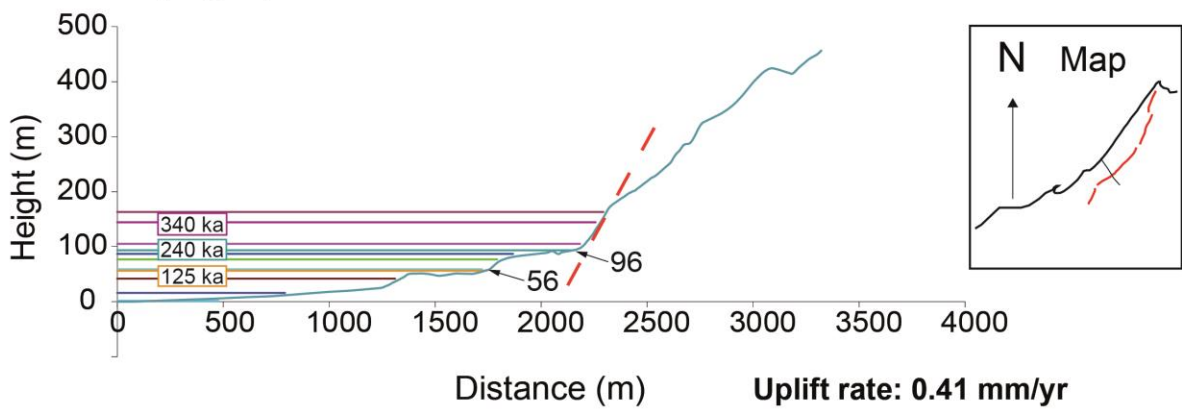
Topographic Profile 6 with modelled shoreline elevations



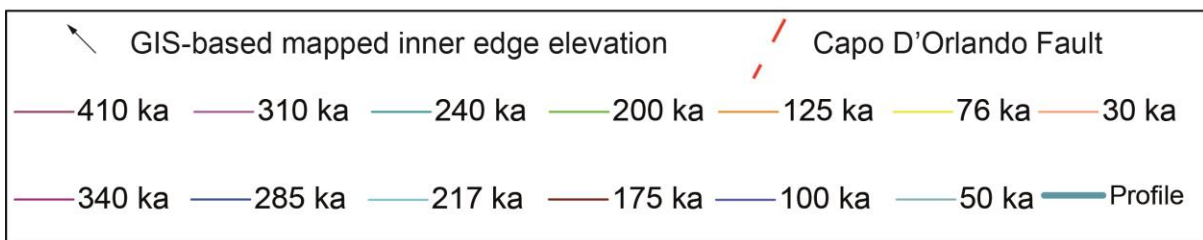
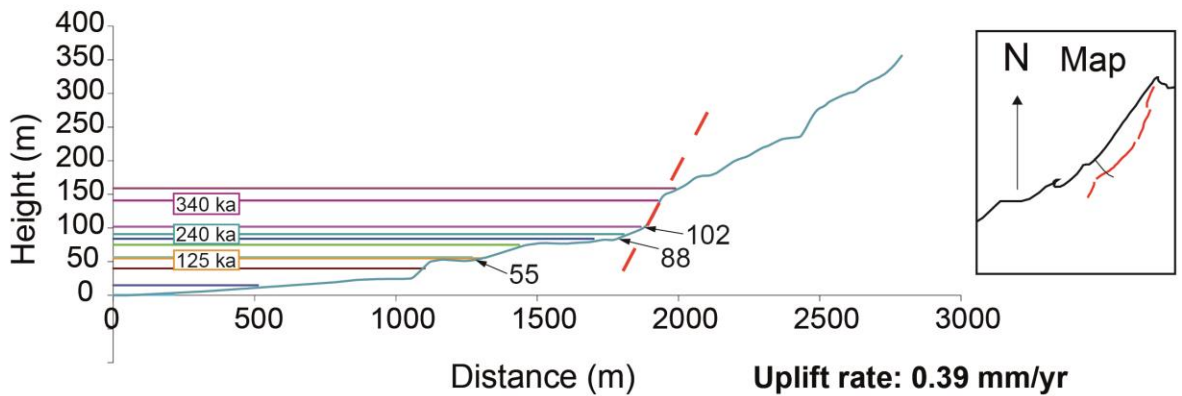
Topographic Profile 7 with modelled shoreline elevations



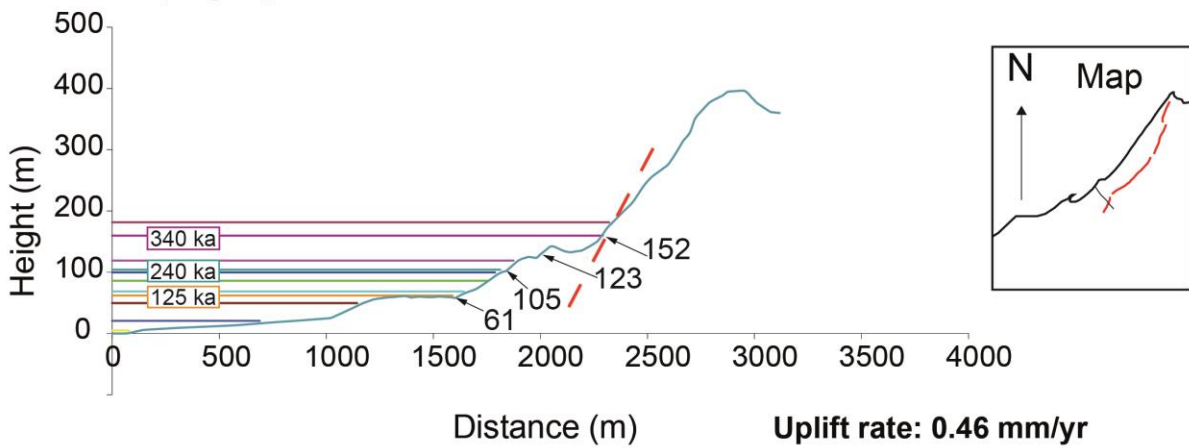
Topographic Profile 8 with modelled shoreline elevations



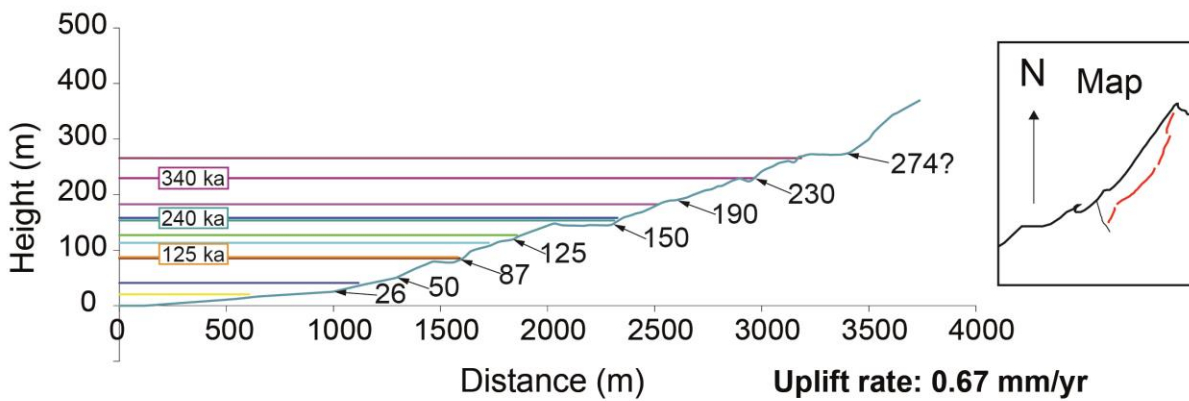
Topographic Profile 9 with modelled shoreline elevations



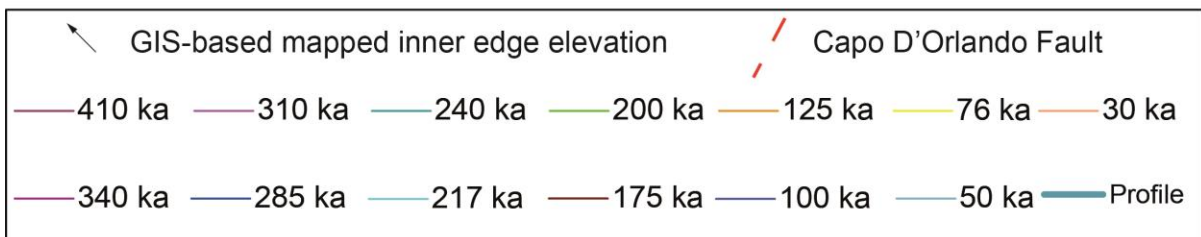
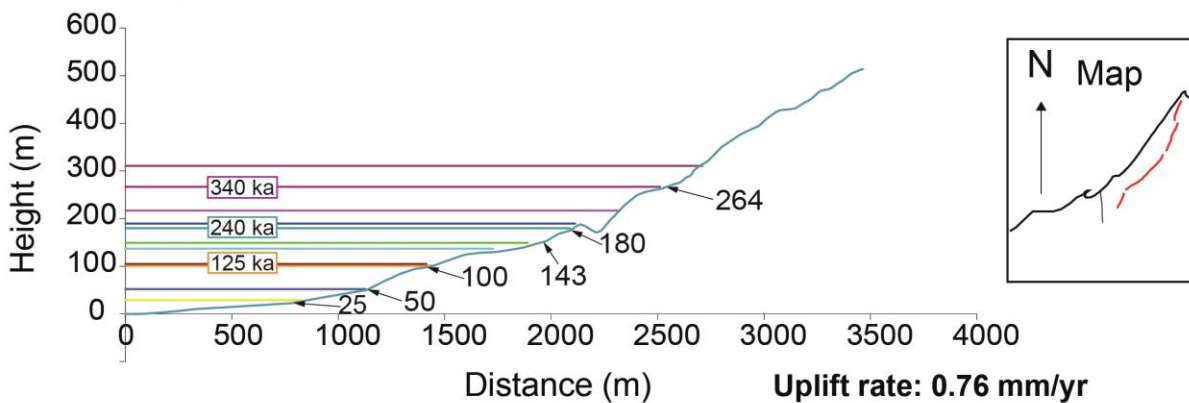
Topographic Profile 10 with modelled shoreline elevations



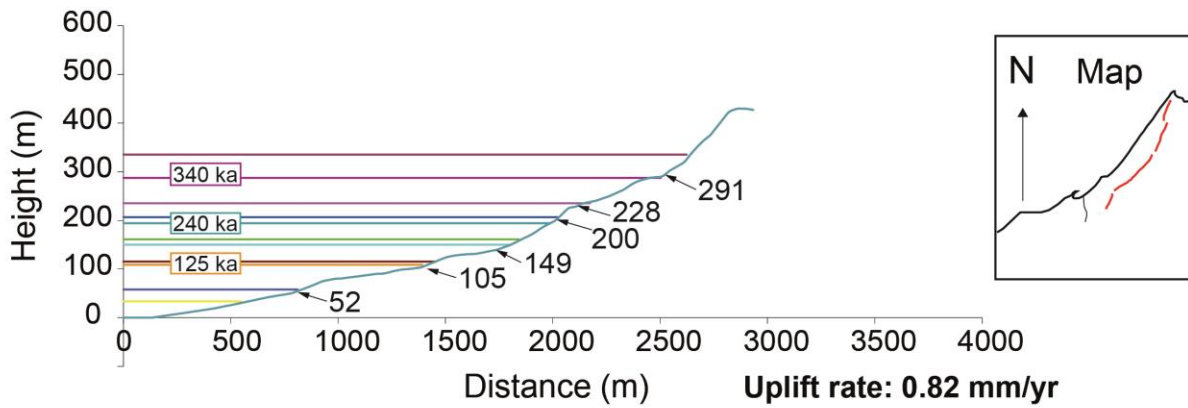
Topographic Profile 11 with modelled shoreline elevations



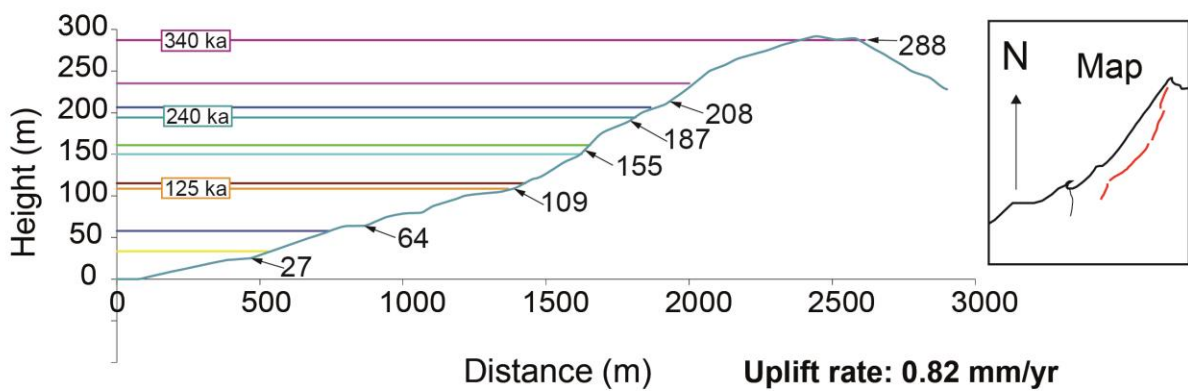
Topographic Profile 12 with modelled shoreline elevations



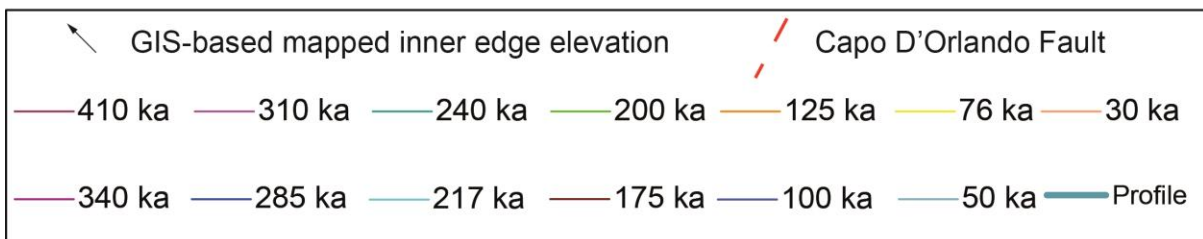
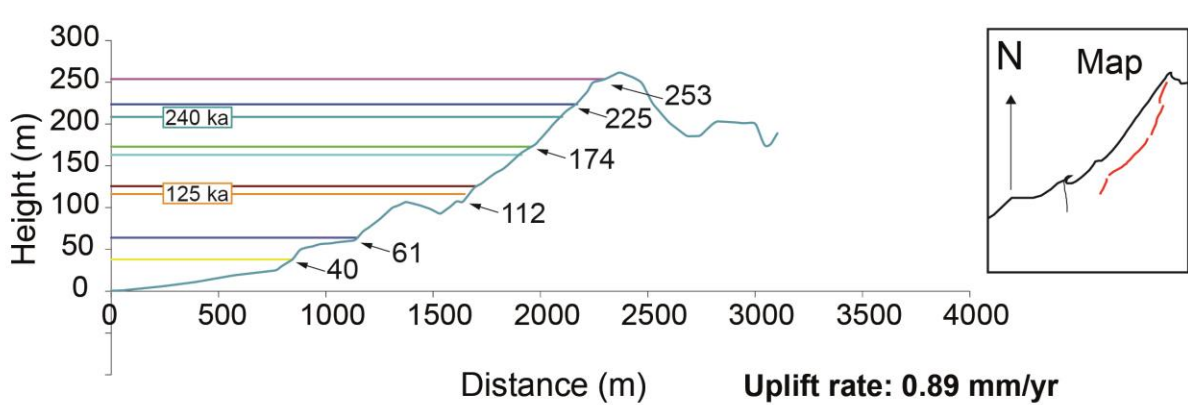
Topographic Profile 13 with modelled shoreline elevations



Topographic Profile 14 with modelled shoreline elevations

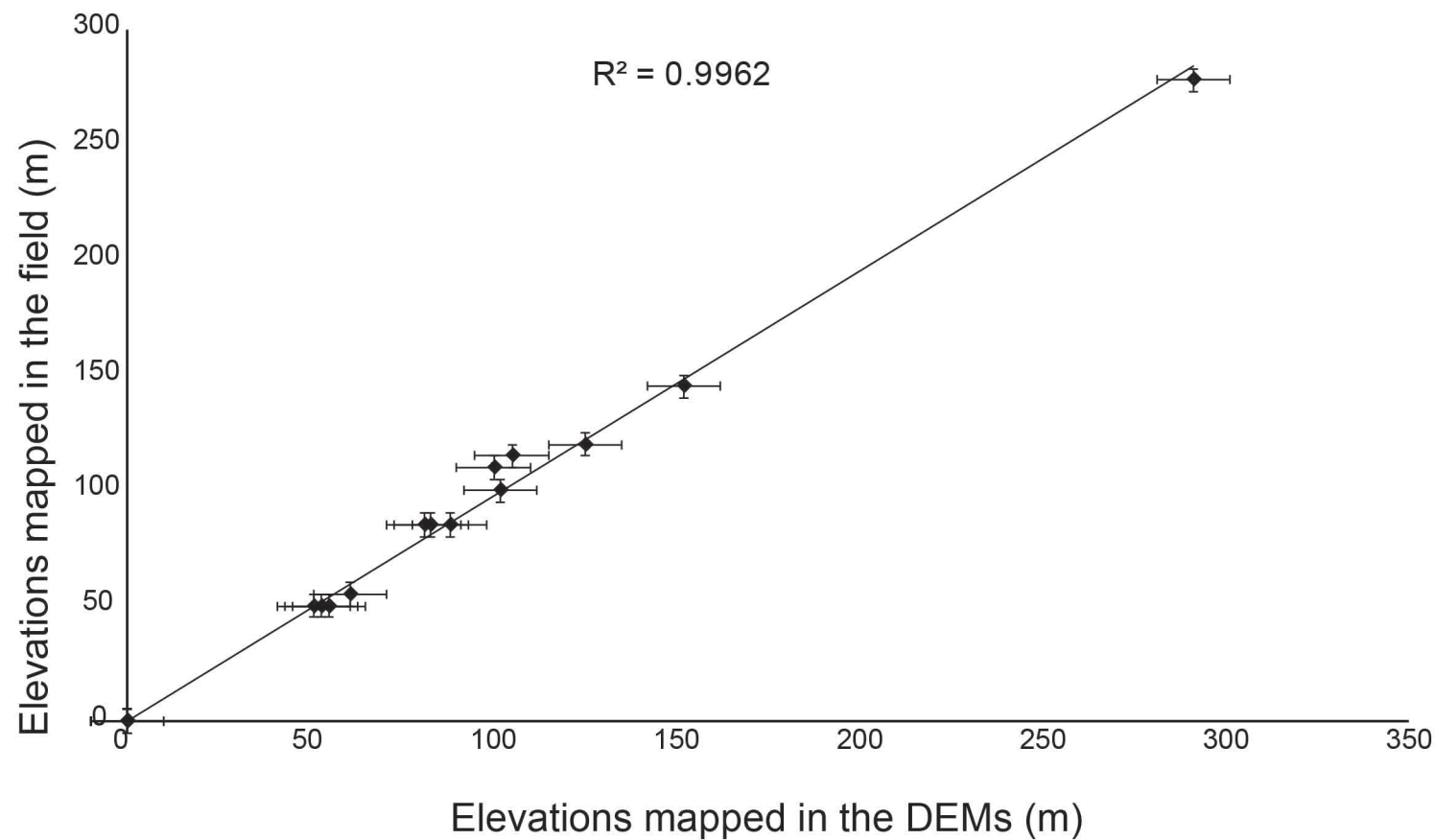


Topographic Profile 15 with modelled shoreline elevations



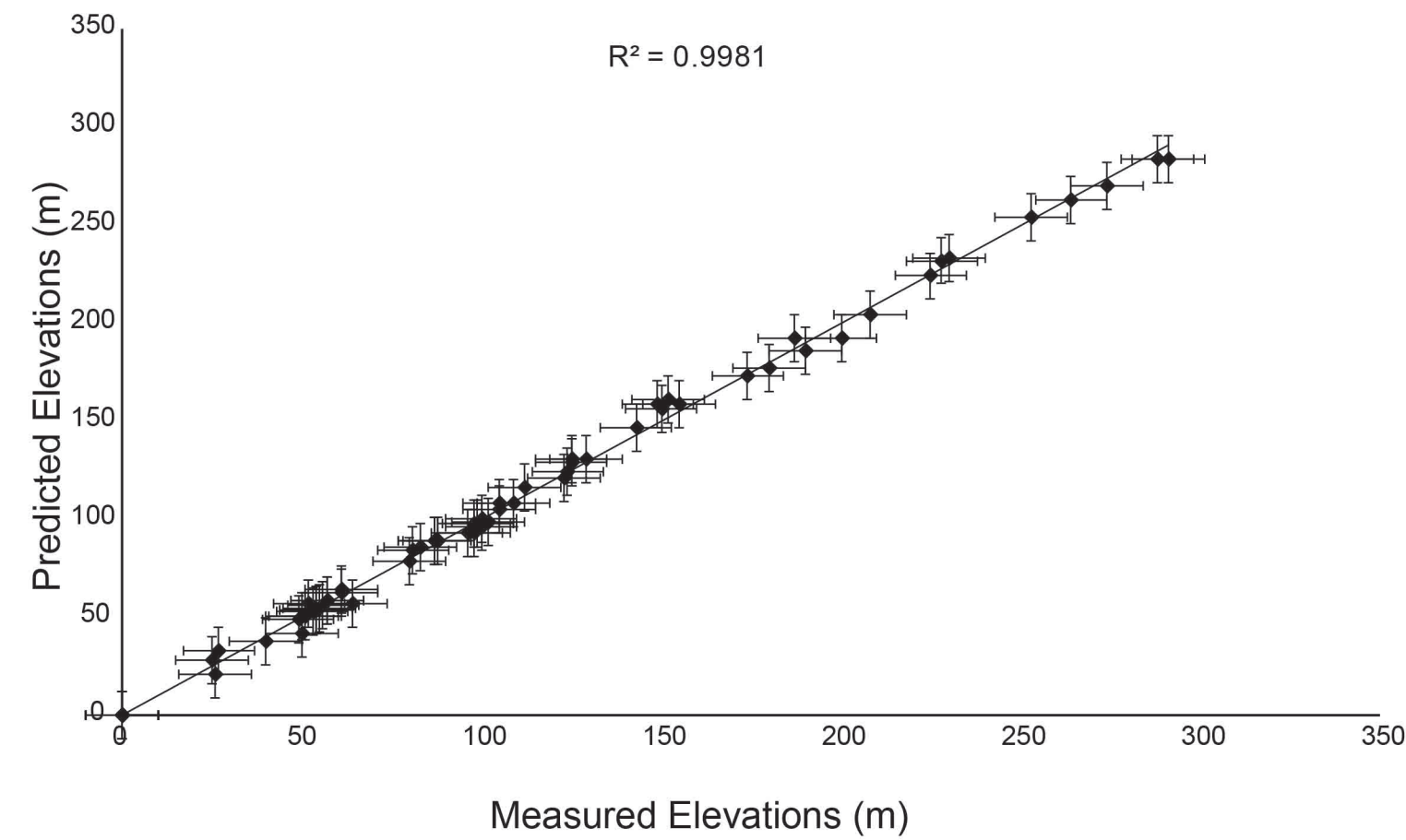
a

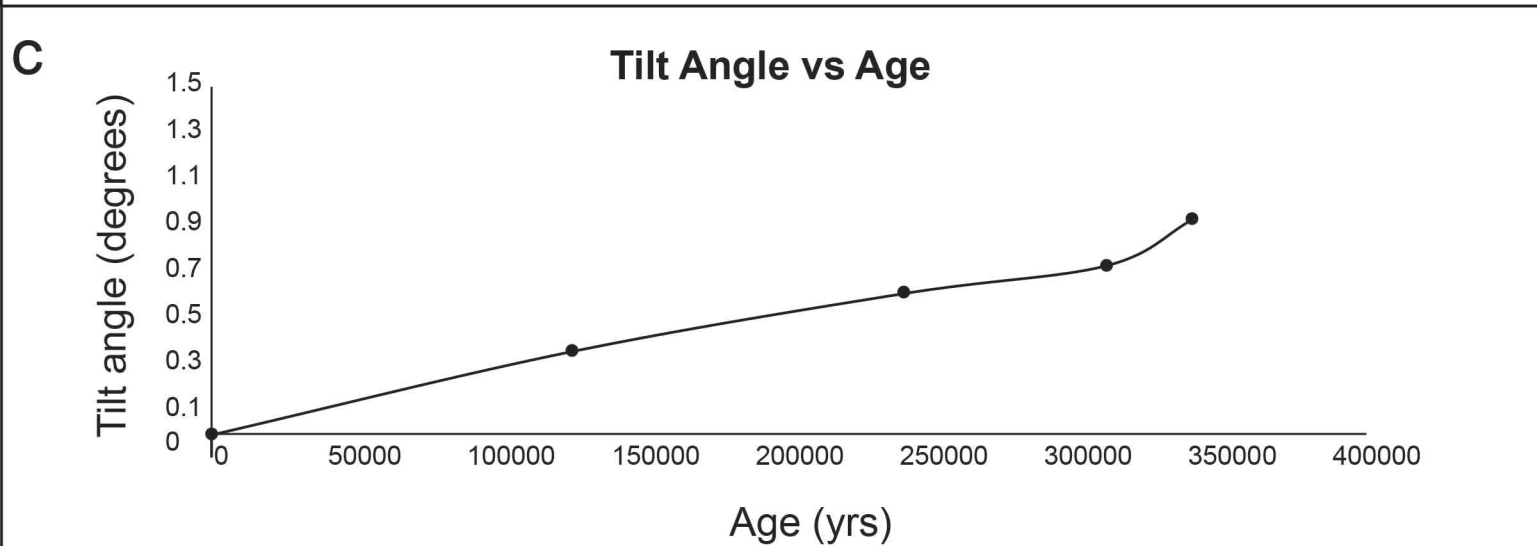
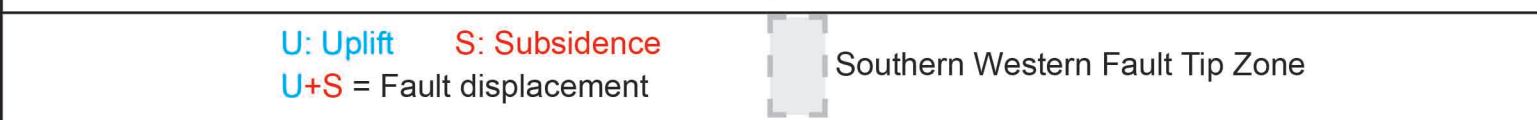
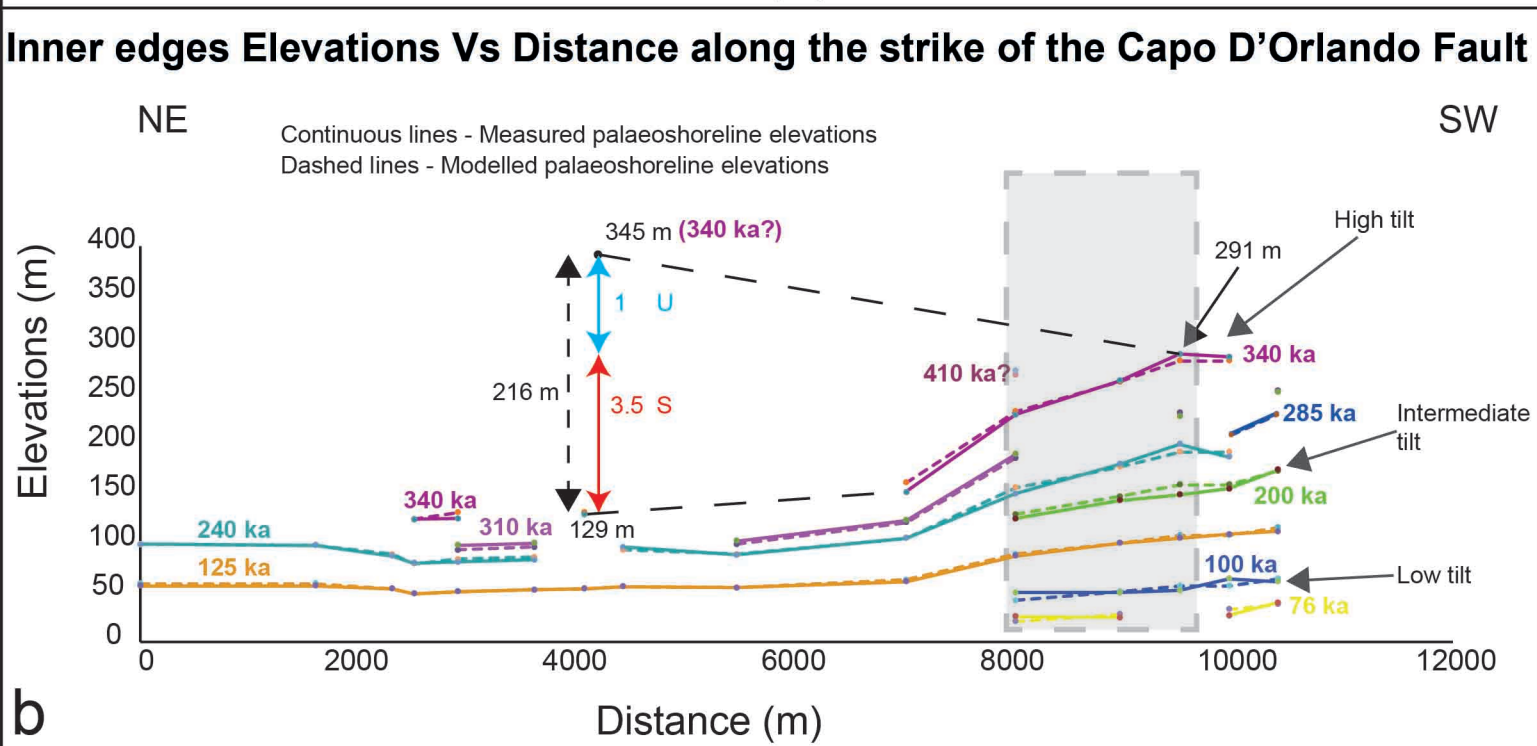
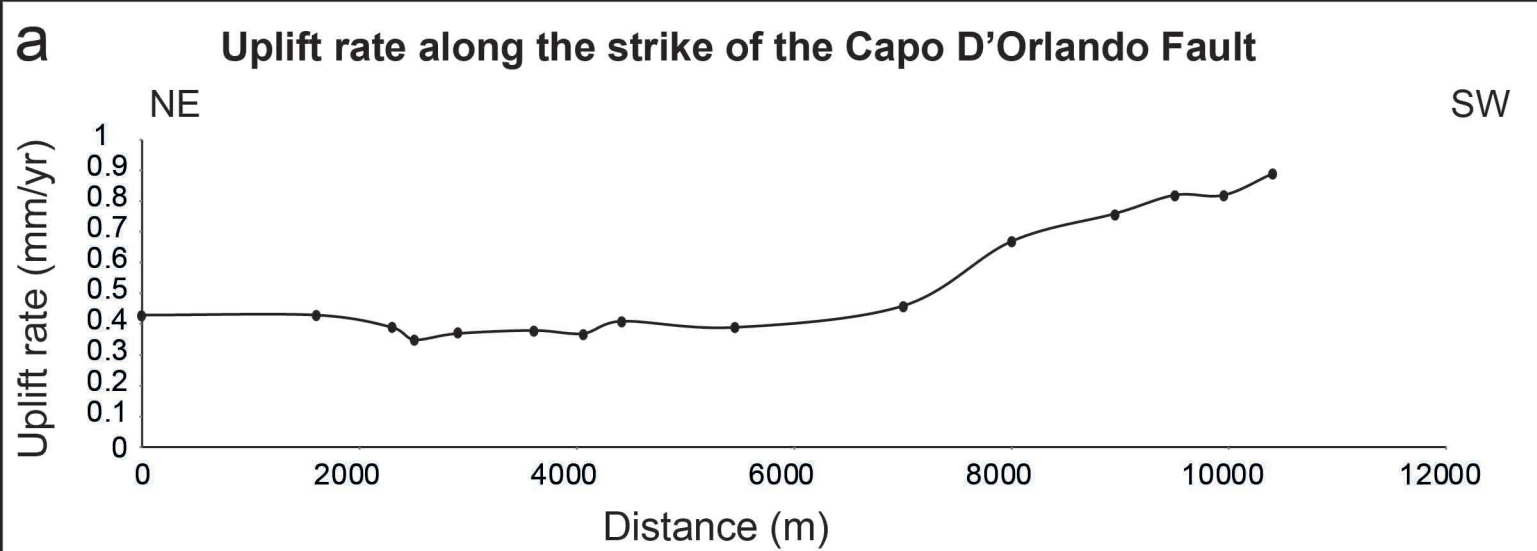
Field-based vs DEMs-based Elevations



b

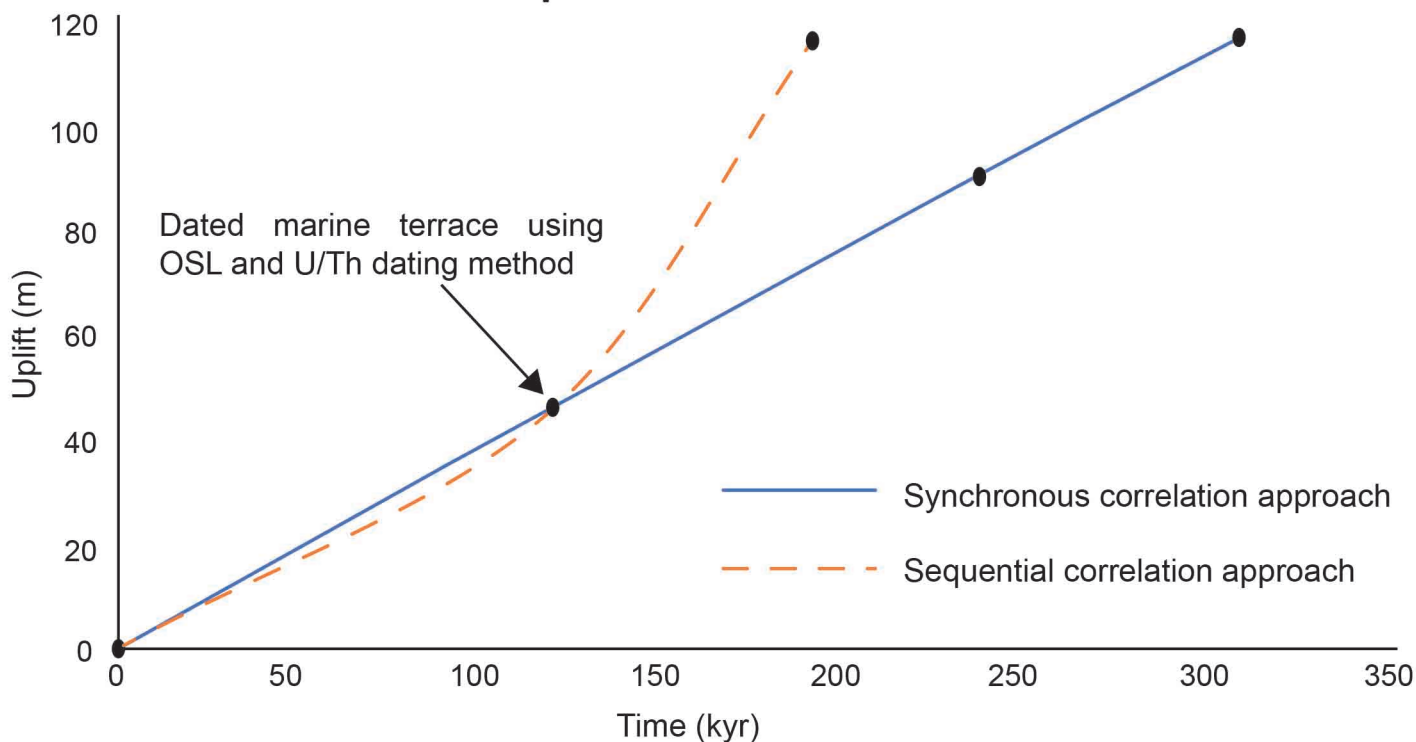
Measured vs Predicted Elevations





a

Uplift vs Time



b

Uplift rate vs Time

